15

The Role of Sintering in the Synthesis of Luminescence Phosphors

Arunachalam Lakshmanan
Saveetha Engineering College,
Thandalam, Chennai,
India

1. Introduction

The phenomena of calcination, roasting and sintering are closely related and often used intermittently. *Calcination* is the process of subjecting a substance to the action of heat, but without melting or fusion, for the purpose of causing some change in its physical or chemical constitution. The objects of calcination are usually: (1) to drive off water, present as absorbed moisture, as "water of crystallization," or as "water of constitution"; (2) to drive off carbon dioxide, sulphur dioxide, or other volatile constituent; (3) to oxidize a part or the whole of the substance. The process of calcination derives its name from the Latin *calcinare* (to burn lime) due to its most common application, the decomposition of calcium carbonate (limestone) to calcium oxide (lime) and carbon dioxide in order to produce cement. In *roasting*, the minerals impose heartburn, which is used to drive out volatile components whereas in *sintering*, small pieces of ore or powder are heated to make bonding. *Sintering* is a method for making objects from powder through agglomeration by heating the material in a furnace to 80-90% of its melting point until its particles adhere to each other. It is known as solid state sintering. The clay particles sinter even before they actually begin to melt into a glassy state (vitrification). The production of powder metal components can be summarized in three steps; powder preparation, compaction and sintering.

Sintering is traditionally used for manufacturing ceramic objects, and has also found uses in such fields as powder metallurgy and synthesis of impurity doped luminescence phosphors. The source of power for solid-state processes is the change in free or chemical potential energy between the neck and the surface of the particle. This energy creates a transfer of material though the fastest means possible; if transfer were to take place from the particle volume or the grain boundary between particles then there would be particle reduction and pore destruction. The pore elimination occurs faster for a trial with many pores of uniform size and higher porosity where the boundary diffusion distance is smaller. Control of temperature is very important to the sintering the process, since grain-boundary diffusion and volume diffusion rely heavily upon temperature, the size and distribution of particles of the material, the materials composition, and often the sintering environment to be controlled. Through diffusion and other mass transport mechanisms, material from the particles is carried to the necks **(Fig.1**), allowing them to grow as the particle bonding enters the *intermediate stage*. The intermediate stage of bonding is characterized by the pores

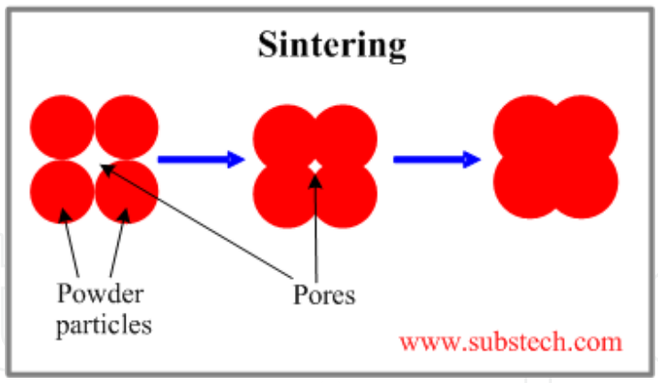

(a)

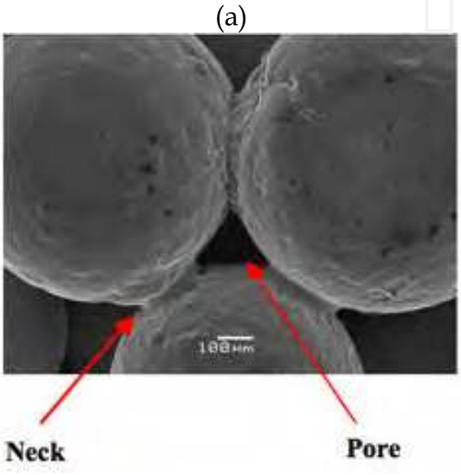

(b)

Fig. 1. (a) Process of sintering (b) The initial stage of the bonding occurs as small "necks" form between the particles.

beginning to round. As the mass transport continues, the pores will become even more rounded and some will appear to be isolated away from the grain boundaries of the particles. This is referred to as the *final stage* of bonding. The final step of the sintering process is to cool the bonded compact to a temperature at which it can be handled. This cooling is performed in an atmosphere that is no longer required to chemically react with the compact. The atmosphere in this stage of the process aids in the transport of the heat away from the compact and minimizes the re-oxidation of the compact during cooling. There are two types of sintering: with pressure (also known as hot pressing), and without pressure. Pressureless sintering is possible with graded metal-ceramic composites, with a nanoparticle sintering aid and bulk molding technology.

Luminescence phosphors owe their practical importance to their property of absorbing incident energy and converting it into visible radiations. This phenomenon, known as luminescence, is driven by electronic processes in the material due to the presence of trapping levels created by the presence of impurity atoms or lattice defects. *Solid-state diffusion* (SSD) reaction is the most popular method used in the synthesis of commercial luminescence phosphors as it is easily reproducible and amenable to large scale production. The products obtained yield a high luminescence efficiency. However, SSD has some disadvantages, such as (1) process complexity and energy-consuming (firing at high

temperature, repetitive heat treatment, milling, and sieving), (2) inhomogeneous mixing and contamination by impurities, (3) product with irregularly shaped and aggregated particles unsuitable for screen brightness and high resolution. Deagglomeration of sintered phosphor chunks is quite cumbersome involving pulverizing, milling, sieving etc. As a result, many attempts have been carried out to find alternative methods for the preparation of phosphors. Superior display performance requires improvement in phosphors particle characteristics such as grain morphology and particle size on the luminescent intensity, efficiency, and resolution. Powders with optimal properties are obtained by different methods such as *chemical precipitation, the sol-gel, solution combustion, plasma chemical, hydrothermal, spray pyrolysis, microwave* etc. However, in most cases, high temperature (although lower than those used in SSD) sintering of samples prepared by these methods was often found to be essential as it increased their luminescence efficiencies due to improved crystallization and optimal incorporation of dopants in the host crystals.

2. Effects of sintering fluxes on morphology

$BaMgAl_{10}O_{17}:Eu^{2+}$ (BAM:Eu) phosphor is an important blue-emitting phosphor and has found widespread applications in plasma display panels (PDPS) and fluorescent lamps. The BAM phosphor powders synthesized with individual flux materials, such as AlF_3, NH_4F, LiF, and so on, have been found to exhibit different morphologies. Flux materials are usually compounds of alkali- or alkaline earth metals with lower melting temperatures than that of the host. In this study, $BaMgAl_{10}O_{17}:Eu^{2+}$ phosphor was prepared with fluxes by spray drying and post-treatment processes. The phosphor prepared with combination of KF and H_3BO_3 resulted in fairly uniform hexagonal plate-like morphology **(Fig. 2),** and the morphology as well as the plate size is actually in between those obtained by each of these fluxes. However, the phosphor prepared with the combination of KF and NaCl gives particles showing two distinct morphologies, including thin hexagonal plates and rounded particles **(Fig. 3).** These morphologies had appeared to be a mixture of the products

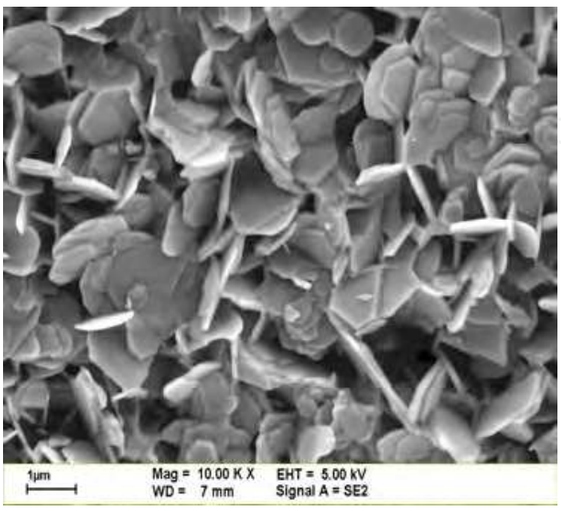

Fig. 2. SEM photographs of the BAM : Eu phosphor prepared with KF and H_3BO_3 **[1].**

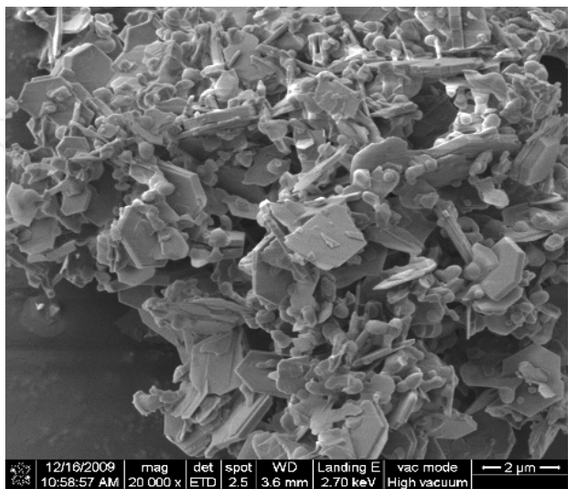

Fig. 3. SEM photographs of the BAM : Eu phosphor prepared with KF and NaCl **[1].**

resulting from each individual of the two fluxes. These powders show different photo-luminescence (PL) intensities. To sum up, by selecting distinct individual or binary fluxes, the morphologies, particle size, and the PL intensities of BAM phosphor can be controlled. Beside, both larger crystal size and appropriate aspect ratio play a crucial role on enhancing the luminescence of BAM phosphor.

3. Role of flux in calcination temperature

$CaAl_2O_4:Eu^{3+},R^+$ (R=Li, Na, K) phosphors were initially prepared by mixing stoichiometric amounts of $CaCO_3$, Al_2O_3 (A.R.), Eu_2O_3 (99.99%), and with or without one of Li_2CO_3, Na_2CO_3 or K_2CO_3 (A.R.) flux using solid state reaction technique at high temperature. Then a certain quantity of flux H_3BO_3 were added. The quantity of the flux H_3BO_3 is very crucial and dictates the calcination and reduction temperatures. The X-ray diffraction patterns of $CaAl_2O_4:Eu^{3+,}$ Li^+ sample (Eu^{3+} and Li^+ were 3 mol.%) calcined at 1000, 1100, 1200 and 1300 °C for 4 h are shown in **Fig. 4**. After calcined at 1000 and 1100 °C, the precipitated precursors showed some characteristic peaks of Al_2O_3 and CaO besides the characteristic peaks of $CaAl_2O_4$. When the temperature was increased to 1200 °C, only the $CaAl_2O_4$ phase was detected (JCPDS card No. 23-1036), and no other products or starting materials were observed. The high intensity of the peaks reveals the high crystallinity of the synthesized

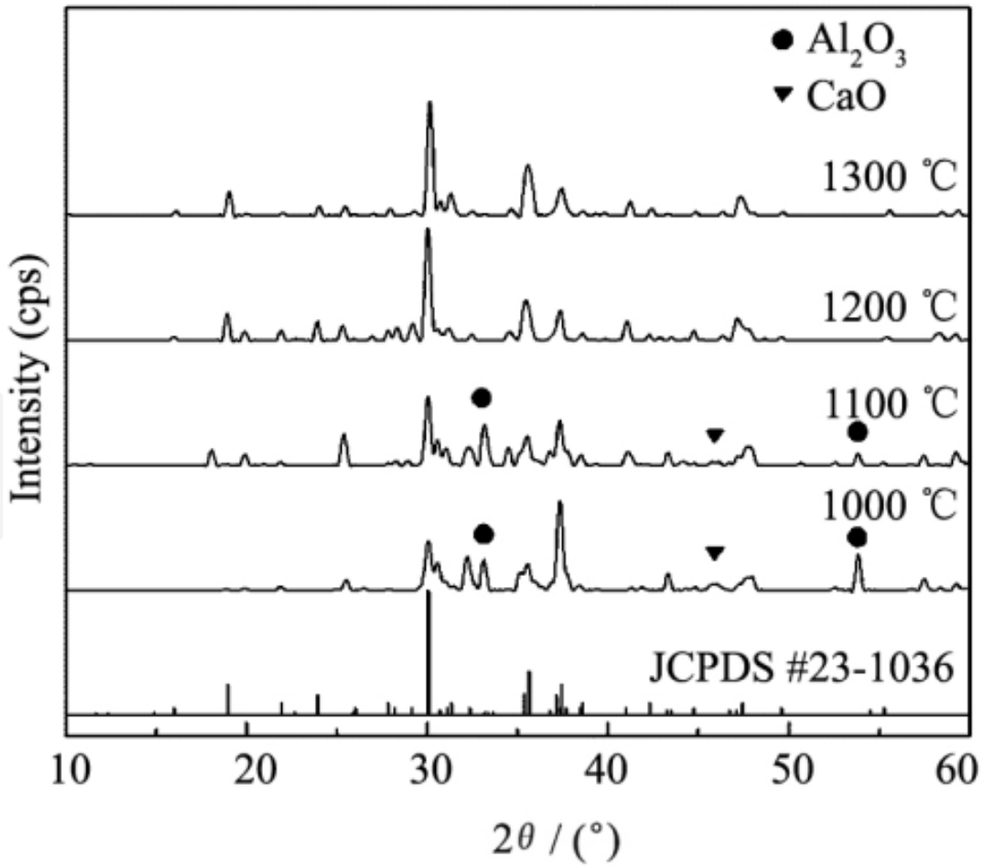

Fig. 4. XRD patterns of $CaAl_2O_4:Eu^{3+,}Li^+$ phosphors sintered at different temperatures **[2].**

powders. The sintering temperature was optimized to be 1200 °C. The luminescence intensity of $CaAl_2O_4:Eu^{3+}$ was significantly enhanced by co-doping with alkali metal ions, probably due to the charge compensation. Furthermore, the emission intensities were gradually enhanced when the radius of R^+ became smaller from K^+ to Li^+ ion. It was probably due to the difference of ionic radii which would give rise to the diversity of sub-lattice structure around the luminescent center ions. This fundamental work might be important in developing new luminescent devices applicable for tricolor lamps, light emitting diodes and other fields.

In Y_2O_3:Eu sintered at 700-1200^{0}C in air, Li_2CO_3 flux was found to: (i) enhance the crystalline growth, ii) improved the grain size slightly morphology from a plate like structure to spherical shape, and iii) improved significantly its PL sensitivity. The optimal red PL was achieved when the $Y_2O_3:Eu^{3+},Li^+$ phosphor was synthesized using 11 mol% Eu_2O_3 and 70 mol% Li_2CO_3 and sintered at 1,200°C for 5 h.

In $ZnWO_4$, the maximum PL intensity was obtained when the sintering temperature was 1,100°C. A significant decrease in PL intensity was measured when the phosphor was sintered at 1,200°C. This decrease was attributed to a change in the crystallinity of the phosphor, in which (020) ZnWO4 was the dominant crystalline phase. Empirically, the change in crystallinity alters the emission mechanisms of the phosphor. The growth of larger phosphor grains was another reason for the decrease in luminescence. Furthermore, the PL spectrum was broadened when the sintering temperature increased. Apparently, oxygen vacancies were involved in the phosphor crystal, and the bluish-green emission was related to electron transitions from the energy levels of the ionized oxygen vacancies to the phosphor valance band. The concentration of oxygen vacancies usually increases with an increase in sintering temperature and a broadened emission is thus observed.

Significantly, on UV illumination, a white-light phosphor could be achieved if the bluish-green $ZnWO_4$ and red $Y_2O_3:Eu^{3+},Li^+$ phosphors were blended.

4. Molten salt sintering

Combined co-precipitation with the molten salt method, a new technology for preparation of $Y_2O_3:Eu^{3+}$ and YAG:Ce^{3+} phosphors was proposed with the controlled size and higher luminescent intensity. With rare earths oxide as raw materials, the molten salt method was compared with solid phase method. Some main principles for the selection of molten salt system were, i) the melting point should lower the temperature of phosphor preparation, ii) the difference of boiling point and melting point should be as wide as possible, and iii) the molten salt must not be hazardous to luminescent intensity. The best multiple molten salt system for $Y_2O_3:Eu^{3+}$ and YAG:Ce^{3+} were NaCl+S+Na_2CO_3 and Na_2SO_4+BaF_2, respectively **[2].** Molten salt sintering improved the crystal degree and configuration of phosphors, resulting in higher luminescent intensity. Using YCl_3 and $EuCl_3$ as raw material, the preparation of $Y_2O_3:Eu^{3+}$ precursor was investigated concerning some factors, such as temperature, complexing agent, precipitation agent and the dripping mode. The size of precursor was the smallest at pH=7 and the complexing agent could control the release velocity of rare ion effectively. With citric acid as a complexing agent, the size of precursor and sintering sample was the smallest and the luminescent intensity of sintering sample was

the highest. Probably, the citric acid could complex effectively the earth ionic and buffer the pH during the precipitation process in the presence of ammonia and therefore enhanced the precursor density and activity. For the preparation of $Y_{3-x}Ce_xAl_5O_{12}$ (YAG:Ce^{3+}) precursor by co-precipitation, the optimal process condition were: the concentration of salt was as low as about 0.05M, precipitation agent was NH_4HCO_3, pH=8, temperature=90℃, and adverse dripping mode was preferred. Because the precursor was a sol mixture of $Y_2(CO_3)$,nH_2O and $NH_4AlO(OH)HCO_3$, it was easy to agglomerate after drying. It was found that the agglomeration problem could be solved by adding active carbon before precipitation. For active carbon, its numerous capillary frameworks might disconnect the sol effectively and its incomplete combustion in sintering was helpful for the deoxidization from Ce^{4+} to Ce^{3+}. Through adjusting components of multiple molten salt and mole ratio of the molten salt to precursor, the optimal sintering conditions for preparation of Y_2O_3:Eu^{3+} and YAG:Ce^{3+} were obtained. The samples were sphere-like particles whose average size were 1~3μm and 3~5μm and luminescent intensity were 11% and 8% better than commercial phosphor respectively. The results for different sintering temperature indicated that molten salt could reduce activation energy of phosphor like a kind of catalyst, leading to lower sintering temperature than solid phase method. The formation of sphere-like particles might be owing to the surface tension difference between liquid molten salt and phosphor, and the existence of double layer insured the dispersion of particles. The liquid molten salt provided the stable high temperature field and liquid environment and promoted the crystal degree, resulted in the increased luminescent intensity. In addition, the mole ratio of Y:Al:Ce was investigated for increasing luminescent intensity of YAG:Ce^{3+}. Luminescent intensity of sample was enhanced evidently when the mole ratio of Y:Al:Ce was reduced from 2.94:5:0.06 to 2.90:5:0.06 in $Y_{3-x}Ce_xAl_5O_{12}$. A little lack of Y in crystal lattice might help to increase luminescent intensity, which coincided with the theory of radiation from crystal lattice defect. The structure of Y_2O_3:Eu^{3+} and YAG:Ce^{3+} was body-centered cubic structure and yttrium aluminum garnet structure respectively showing that the molten salt did not enter into the crystal lattice of phosphor. Compared with the traditional solid phase method, the new technology can obtain the controlled size and higher luminescent intensity phosphor through only one sintering process, avoiding comminuting process required in solid phase method. In addition, it is a new energy-saving process with lower sintering temperature and has a potential application in preparation of phosphor with excellent performance.

5. Thermal stability against sintering and crystal structure

The thermal stability of $BaAl_2Si_2O_8$:Eu^{2+} (BAS:Eu^{2+}) phosphor used in PDP was found to depend on its polymorph property - hexagonal and monoclinic crystal structure. The monoclinic BAS:Eu^{2+} when baked at 500 °C in air for 30 min, showed the same PL intensity as the fresh one, whereas the baked hexagonal one lost its PL intensity significantly **(Fig.5)**. Electron spin resonance studies on Eu^{2+} and Rietveld refinement showed that the difference of thermal stability between hexagonal and monoclinic BAS:Eu^{2+} could be ascribed to both the crystal structure of host materials and the average inter-atomic distances between the Eu^{2+} ion and oxygen which plays the key role of shield for Eu^{2+} ions against an oxidation atmosphere.

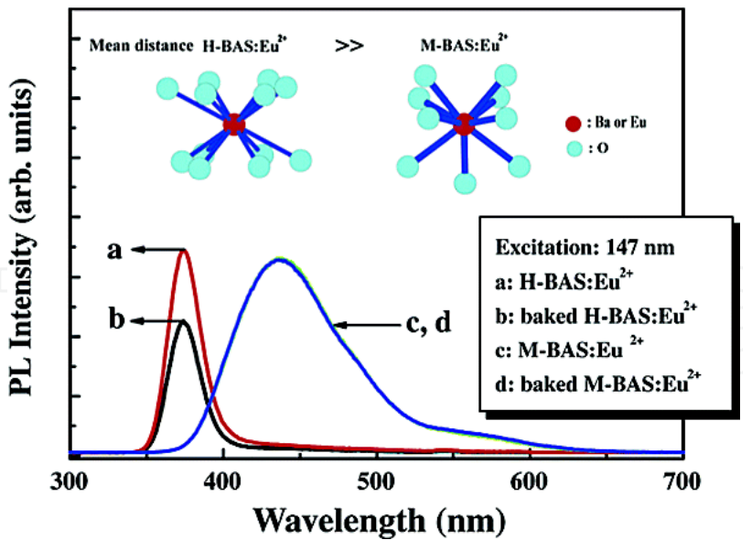

Fig. 5. Emission spectra of $BaAl_2Si_2O_8:Eu^{2+}$ ($BAS:Eu^{2+}$) phosphor under VUV (147 nm) excitation **[3]**.

6. Effect of sintering on photo and thermo-luminescence in $CaSO_4$: Dy phosphor

Sieving *before* the high-temperature sintering treatment has successfully eliminated particle agglomeration during subsequent sintering, and has further enhanced its thermoluminescence (TL) sensitivity to γ-rays. The reduction in TL sensitivity of higher sized grains observed following the procedure of sieving *after* sintering has also more or less vanished. Maximum TL sensitivity is seen after sintering around 700°C, whereas maximum PL sensitivity is seen after sintering around 325°C. While the observed increase in TL sensitivity (by 30%) with increasing sintering temperature in the range 325-700°C is explained on the basis of diffusion of Dy^{3+} ions from the surface to the whole volume of the grains (0-75 μm), the drastic decrease (by a factor of 3) in PL sensitivity with increasing sintering temperature is explained on the basis of change in the Dy^{3+} environment on the grain surface perhaps due to oxygen incorporation **(Fig.6)**. Washing with water and acetone, which affect mainly the surface traps, enhances the PL sensitivity of $CaSO_4$:Dy slightly; however, it does not influence TL sensitivity very significantly. Grinding reduces PL in general, but no such trend was noticed in TSL which supports the conclusion that PL originates mainly from surface traps since grinding affects mainly the grain surface. However, the sharp reduction in TL and PL sensitivities observed at 400°C indicates that an unusual process takes place near that sintering temperature. TG-DTA (thermogravimetric and differential thermal analysis) data indicate that dysprosium sulphate dopant in $CaSO_4$ which are hydrated at RT become anhydrous at 400^0C and the water molecules released possibly damage the crystal lattice which get restored at higher sintering temperatures. As a result, $CaSO_4$:Dy annealed at 400^0C show a slightly reduced TL while those annealed at 300^0C or at 700^0C do not show any such reduction. The water molecules released at 400^0C possibly displace Dy from its lattice site causing a reduction in TL. No such reduction in TLis observed on annealing at 300^0C since the water molecules do not get dislodged from the lattice. Annealing at 700^0C possibly restore the Dy in its original lattice sites and hence restore the TL sensitivity.

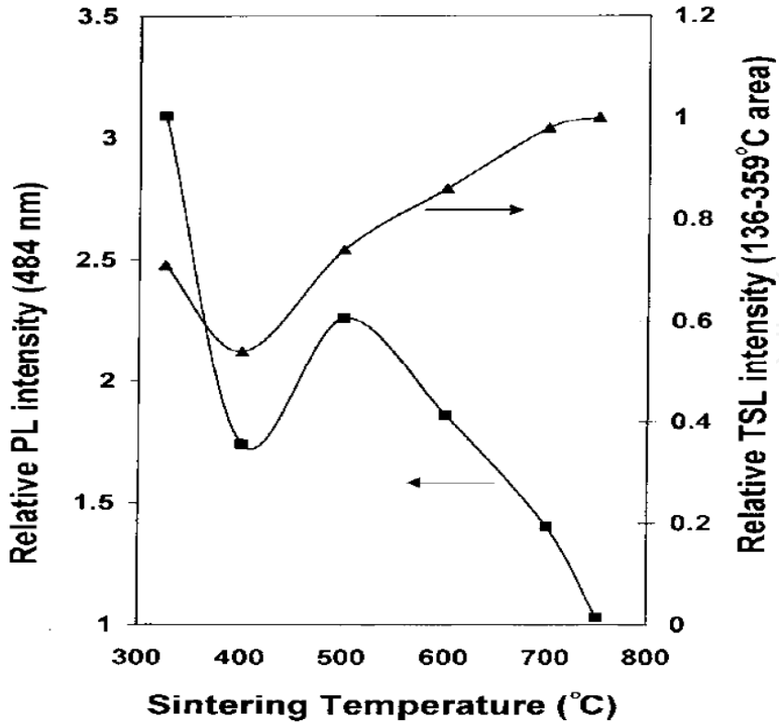

Fig. 6. Dependence of the Thermostimulated luminescence (TSL, 136–359°C area) as well as 484 nm PL emission (λ_{exi} = 350 nm) intensities of unwashed as prepared samples (<75μm grain size and sieving carried out before sintering) of $CaSO_4$:Dy on the sintering temperature **[4].**

7. Precipitation and sintering – TG/DTA studies

Eu^{2+} activated long lasting $Sr_4Al_{14}O_{25}$ nano sized phosphor synthesized by precipitation method is a revealing study. $Al(NO_3)_3$ $9H_2O$, $Sr(NO_3)_2$, $(NH_4)_2CO_3$, $Eu(NO_3)_3$ and $Dy(NO_3)_3$, all in analytical purity, were the starting materials. The $(NH_4)_2CO_3$ solution was added in droplets to produce a white precursor. After drying at 120°C for 24 h, the final luminescent powders were obtained by calcinating the dried precursor at different temperature from 1200 to 1300 °C in a reducing environment of 5%H_2 + 95%N_2. Thermogravimetric (TG) and differential thermal analysis (DTA) studies revealed that the endothermic peaks A and B in DSC (differential scanning calorimetry) curve can be assigned to the dehydration of $Al(OH)_3$ and the other two endothermic peaks C and D can be assigned to the decomposition of $SrCO_3$, since the dehydration usually occurs at a relatively low-temperature. The TG curve also shows a good accordance with the DSC result. It can be seen from the TG curve that the weight loss (WL) after the dehydration is 20.6%, very close to the theoretical value 22.5%. And the weight loss after the decomposition of the carbonate is 10.2%, which is also very close to the theoretical value 10.5%.It is obvious that the TG curve reveals no weight loss after 1100°C, indicating that the two exothermic peaks E and F may result from the chemical reaction between the calcined oxides at high-temperature. XRD data reveal the formation of the orthorhombic aluminate could take several steps, and the low-temperature products after the dehydration and decomposition, say Al_2O_3 and SrO, will react spontaneously to formthe monoclinic $SrAl_2O_4$ around 1200°C. When the calcination temperature increased to

1250°C, some peaks of new phases, $SrAl_{12}O_{19}$ and $Sr_4Al_{14}O_{25}$, are identified from the XRD pattern, showing the complex of the phase transition in this temperature region. However, with the calcination temperature increasing to 1300°C, almost all the diffraction peaks can be indexed to the orthorhombic $Sr_4Al_{14}O_{25}$ phase when referring to PDF 74-1810, implying that $SrAl_2O_4$ and $SrAl_{12}O_{19}$ can be viewed as the intermediate phases during the process of $Sr_4Al_{14}O_{25}:Eu^{2+},Dy^{3+}$ preparation. $Sr_4Al_{14}O_{25}:Eu^{2+},Dy^{3+}$ phosphor exhibited better afterglow property than the $SrAl_2O_4:Eu^{2+},Dy^{3+}$ phosphor due to a deeper trap level and a higher trap concentration formed in the host material. When compared to the powder obtained in conventional method, the nano sized powders revealed a blue shift in emission spectrum due to the decrease in grain size **(Figs.7-10)**.

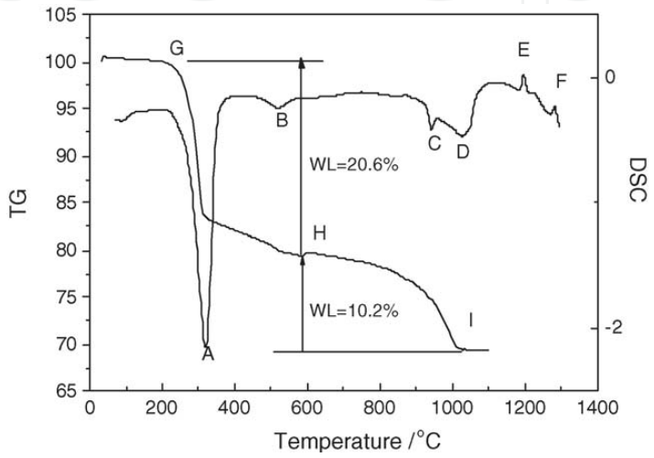

Fig. 7. DSC and TG profiles of precursors, showing the dehydration/decomposition reaction process during calcinations. Note- **DTA** detects any change in all categories of materials; **DSC** determines the temperature and heat of transformation **[5].**

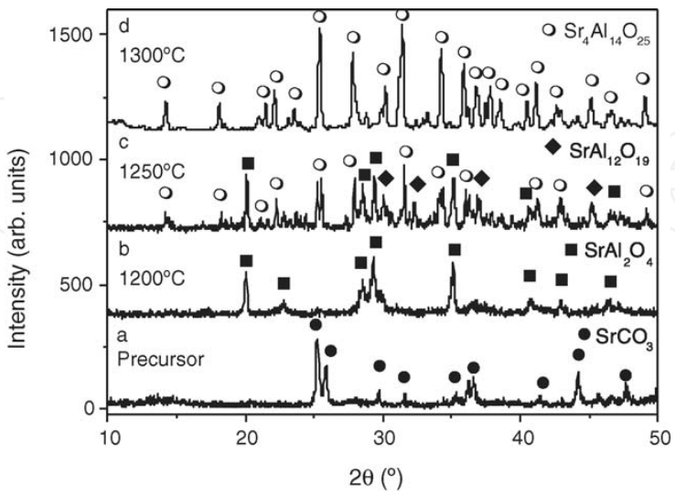

Fig. 8. XRD patterns of the precursors calcined at different temperature: (a) raw powder, (b) 1200 ◦C, (c) 1250◦C and (d) 1300 ◦C, indicating the phase transformation during the calcinations **[5].**

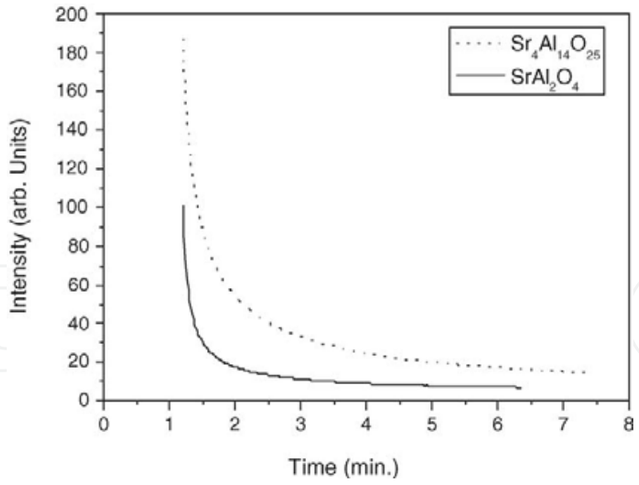

Fig. 9. Afterglow property of the nano scaled phosphors **[5].**

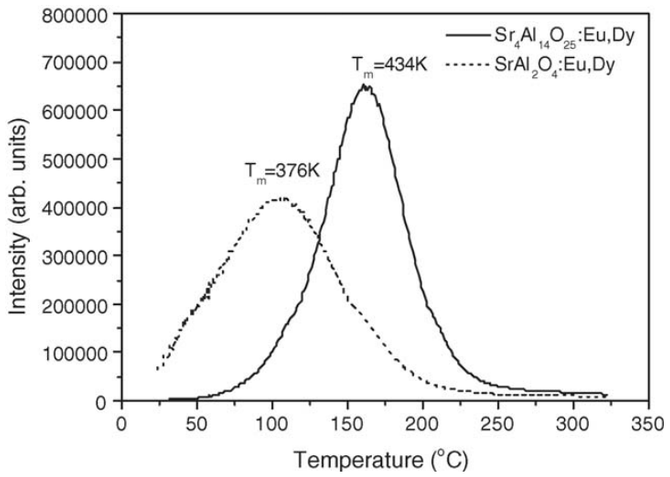

Fig. 10. TL curve for nano scaled $SrAl_2O_4$:Eu,Dy and $Sr_4Al_{14}O_{25}$:Eu,Dy phosphors **[5].**

8. Pelletization and sintering

The change in TL properties due to compression and subsequent heating are well studied in LiF TL dosimetry phosphor. Changes in TL at contacts and in the vicinity of ores in carbonate host rocks and near faults have been studied. In the history of formation of terrestrial planets, the collision of solid bodies is central at an early stage of their evolution. Analysis of shock processes in natural minerals play an important role in geology. Influence of thermal history, deformation and stresses associated with major tectonic dislocations, meteoritic craters and underground nuclear explosions on the TL of several natural minerals have been discussed earlier. Shock-induced TL in Oligoclase, Quartz and Calcite have been studied in this regard. An enhancement in TL intensity and shifting of the glow peaks to relatively higher temperatures in pelletized kyanite samples when compared to single crystals which were attributed to the particle nature of the phosphor and/or pressure-induced defects. A shift in the temperature of glow peaks of γ- and X-ray irradiated quartz with pressure was attributed to an electron trap that is getting shallower with increasing pressure.

During the preparation of sintered pellets for applications in radiation dosimetry, Mg-doped LiF phosphors compressed with a pressure of 100 atm (10.13MPa) exhibited a significant glow curve change and a TL sensitivity decrease by a factor of about 10–16. Phosphors finely crushed in a mortar did not exhibit such a behavior. These changes are reportedly caused due to lattice deformations generated by the static pressure. The deformations quench the original TL peak near 200^0C but produced new traps giving rise to peaks between 230 and 400^0C. Pressure applied to the irradiated phosphor empty the filled traps and create new traps. However, the original glow curve shape and TL sensitivity were restored when the LiF phosphor was heated to a temperature higher than 200^0C even for a shorter period. The sintered pellets were found reusable after a 400^0C, 1h+ 80^0C, 4 h annealing treatment. Subsequent investigations revealed that the pressure-induced defomation disappears fully only when the annealing temperatures are above 350°C; annealing temperatures higher than 100°C cause further complicated variations in the glow curve shape of LiF-based phosphors. Plastic deformation of LiF:Mg,Ti followed by irradiation decreased the TL intensities, with 200^0C peak decreasing more drastically than 100^0C peak. The latter reported that it is more likely that new TL traps are created by dislocation intersections which then compete with the previously existing traps. Plastic deformation after exposure to ionizing radiation increase the F band (250 nm) absorption in LiF:Mg,Ti, while decreasing the absorptions at 310 and 380 nm which are related to TL traps. The rate of change with deformation of the three bands indicates that F-centres are created when 310-and 380-nm absorption centres are destroyed. These results were interpreted in terms of the removal of F-centres from the defect complexes causing the 310- and 380-nm absorption bands.

Studies by the author **[6]** showed pressure-induced changes in the luminescent properties of gypsum ($CaSO_4.2H_2O$), calcite ($CaCO_3$), $CaSO_4$:Dy and anhydrite ($CaSO_4$). A systematic reduction in the TL as well as PL (in the case of $CaSO_4$:Dy) sensitivity with the pressure applied is seen with the former three materials **(Fig.11).** However, an exactly reverse trend,

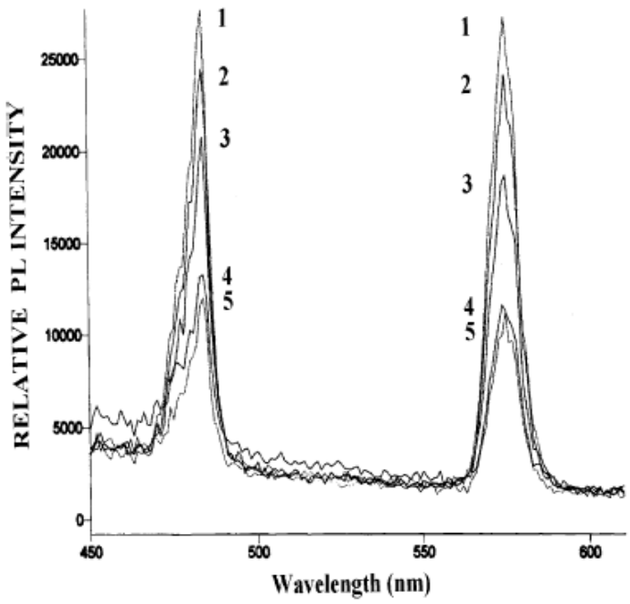

Fig. 11. Dependence of PL emission spectra (λ_{exi} = 350 nm) of unirradiated $CaSO_4$:Dy on the pressure applied (in MPa), 1:0, 2:0.7, 3:1.05, 4:1.23, 5:1.4.**[6].**

i.e., a systematic increase in the TL sensitivity with the pressure was witnessed in the case of anhydrite. While the application of pressure (7MPa) reduced the TL sensitivity of $CaSO_4$:Dy to 43% of its initial value, a 700°C, 1 h anneal could restore its value to only 51%. This shows that the pressure-induced changes are more or less permanent, unlike the case reported with LiF. No change in the XRD data was seen in all these samples on the application of pressure (7MPa) which shows that the changes observed in TL and PL should be attributed to the damage (in the cases of calcite, gypsum and $CaSO_4$:Dy) / creation (in the case of anhydrite) of traps / luminescent centres rather than to the damage to their crystal structure. Pressure applied before or after the irradiation produced no difference in $CaSO_4$:Dy. However, in γ-ray exposed anhydrite and gypsum, pressure-induced changes in the TL sensitivity were quite complex though no change in its glow curve structure was seen. Results showed that in anhydrite, there is a competition between two opposing pressure-induced phenomena—one is radiation damage to the filled traps and the other is the increased luminescence efficiency.

9. Activator diffusion during sintering

$CaSO_4$ can be pelletized only with suitable additives. However, Dy^{3+} could be incorporated in $CaSO_4$ lattice only by recrystallization in H_2SO_4 medium. A recent study **[7]** has shown that Li coactivator could be successfully introduced in $CaSO_4$:Dy/Tm at a concentration of 0.06% during a subsequent step of cold pressing at RT and sintering of the pellets at 700°C. A number of alternative lithium compounds have been used in this role and they include Li2CO3, LiCl, LiF, Li2B4O7 and Li2SO4. Addition of lithium significantly shifted the major TL peak of $CaSO_4$:Dy/Tm from 220°C down to 120°C. The fact that similar results were obtained earlier with Li coactivator added during initial crystal growth show that certain impurities can easily diffuse into host crystal during pelletization followed by sintering. In this case Dy^{3+} incorporation in Ca^{2+} sites creates cation vacancies into which Li^+ co-dopant

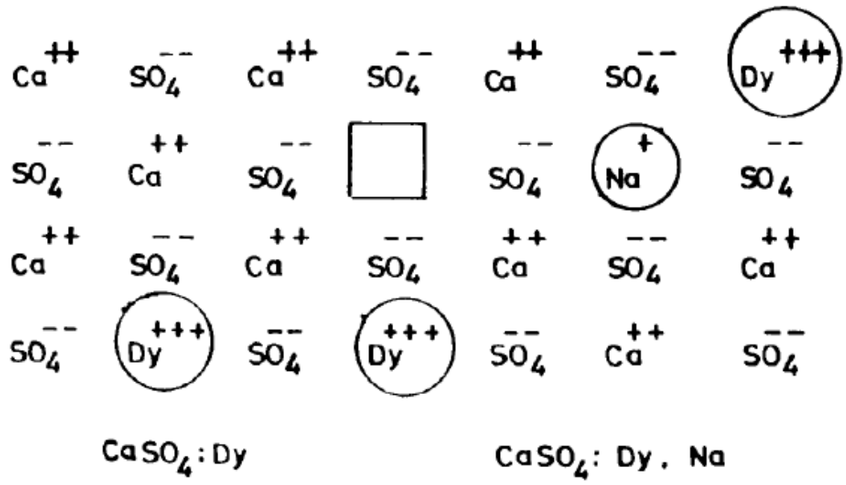

Fig. 12. Pictorial representation of $CaSO_4$:Dy and $CaSO_4$:Dy,Na. Trivalent Dy could be incorporated into $CaSO_4$ lattice only by recrystallization in H_2SO_4 medium. Monovalent co-dopants such as Na^+ or Li^+ could, however, be incorporated into CaSO4:Dy lattice by cold pressing followed by sintering [8].

could easily diffuse in. Such a technique could offer an easy recipe for the preparation of doped samples. Unlike the case with Li co-dopant, Dy^{3+} or Tm^{3+} could not be doped by this (pelletization followed by sintering) technique. This indicates that incorporation of trivalent dopants require greater activation energy than monovalent co-dopants. This is understandable since trivalent dopants in a divalent host require activation energy for the creation of cation vacancies **(Fig.12).**

10. Effect of atmosphere during sintering

Phosphors tend to get oxidised during sintering in air. For example $CaSO_4$ gets oxidized to CaO at temperatures above 800^0C in air. As a result the luminescence efficiency of $CaSO_4$:Dy gets reduced at high sintering temperatures. In addition there are certain activators such as Mn, Cu etc which tend to get oxidised during sintering in air. Certain other activators such Eu and Ce tend to exhibit dual valence state. Quite often during sintering, reducing atmosphere is essential to prevent Eu^{2+} and Ce^{3+} from getting oxidized to Eu^{3+} and Ce^{4+}, respectively. While phosphors containing Eu^{2+} activator (eg., BAM:Eu^{2+}) gives intense blue emission, those containing Eu^{3+} activator (eg., Y_2O_3:Eu^{3+}) gives intense red emission. So depending on the phosphor and activator, sintering should be carried out either in a reducing atmosphere or in air. Reducing atmospheres are usually obtained with H_2/N_2 mixture. Alternately, the phosphors to be sintered are covered with carbon powder in closed crucibles so as to create reducing CO atmosphere when burnt with limited oxygen.

CaS:Eu^{2+} red-emitting phosphors particles, were prepared by the precipitation method with calcium acetate and Na_2S as starting materials, followed by sintering in the atmosphere over the mixture of sulfur powder, Na_2CO_3, and carbon-containing compounds such as tartaric acid, citric avid, glucose, and cane sugar. CaS:Eu^{2+} particles without additive show inhomogeneous, rough and aggregation with the size of 75–125 nm, but the spherical particles with mean size of about 110 nm were obtained by adding carbon-containing compounds **(Fig.13).** Compared with phosphor without additive, the addition of carbon-containing materials induced a remarkable increase of PL, in the order of cane sugar, glucose, citric acid, and tartaric acid. This enhancement is due to the improvement of crystallinity, particle morphology and size distribution of the samples by adding carbon-containing additive.

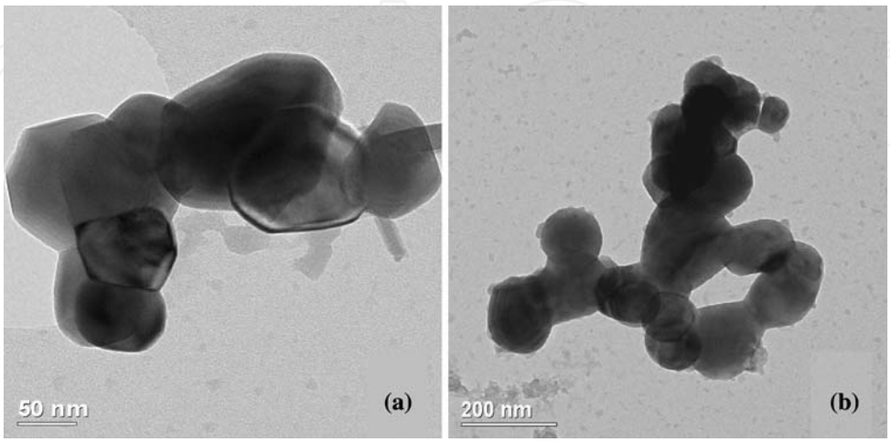

Fig. 13. Transmission electron (TEM) micrographs of CaS:Eu^{2+} obtained by the precipitation method without additive (a) and with cane sugar additive (b) **[9].**

Yttria-stabilized zirconia (YSZ) is a zirconium-oxide based ceramic, in which the particular crystal structure of zirconium oxide is made stable at room temperature by an addition of yttrium oxide. These oxides are commonly called "zirconia" (ZrO_2) and "yttria" (Y_2O_3), hence the name. The addition of yttria to pure zirconia replaces some of the Zr^{4+} ions in the zirconia lattice with Y^{3+} ions. This produces oxygen vacancies, as three O^{2-} ions replace four O^{2-} ions. It also permits yttrium stabilized zirconia to conduct O^{2-} ions, provided there is sufficient vacancy site mobility, a property that increases with temperature. This ability to conduct O^{2-} ions makes yttria-stabilized zirconia well suited to use in solid oxide fuel cells, although it requires that they operate at high enough temperatures.

11. Effect of calcination temperature

Rare-earth ions can easily replace yttrium ions because their properties are similar. All peaks in XRD pattern of $YInGe_2O_7$ doped with 5 mol.% Eu^{3+} and calcined at various temperatures from 1100^0C to 1400^0C in air for 10 h could be attributed to the monoclinic $YInGe_2O_7$ phase. Trivalent europium ions (94.7 pm) were introduced to substitute trivalent yttrium ions (90 pm) in the (Y, Eu) $InGe_2O_7$ system. The variations are almost the same for Eu^{3+} and Y^{3+} ion radii, both easily forming a solid solution. Additionally, there were no charge compensation issues when Eu^{3+} ions substituted Y^{3+} ions in the $YInGe_2O_7$ lattice because both have the same valence. The full-width at half-maximum (FWHM) of these peaks seemed to decrease and the crystallinity of $YInGe_2O_7$:Eu^{3+} became better with an increase of the calcination temperature to 1200^0C. From Fig.14 it is observed that the emission intensity increases with calcination temperature, with a maximum value at1200^0C.

This was caused by the reduction of nonradiative recombination effects, i.e., quenching sites and surface defects trapped by increased crystallinity and decreased defects in the crystal and is in agreement with the results of the XRD analysis, as optimum crystallinity was presented at 1200^oC. Higher calcination temperature enhances atomic mobility and causes grain growth, resulting in better crystallinity. When calcination temperature increased further, the emission intensity decreased significantly as shown in **Fig.14.** When the calcination temperature was higher than 1200^0C, the second phase of In_2O_3 (JCPD no. 06-0416) was observed in the XRD pattern. The amount of the second phase increased with calcination temperature. The second phase might be produced because the increased calcination temperature leads to a nonstoichiometric system because the melting point of In_2O_3 (850^0C) is lower than that of Y_2O_3 (2410^0C) and GeO_2 (1086^0 C).

For the preparation of $ZnWO_4$ phosphor, ZnO powder used as the source material was mixed with WO_3 (99.9%) at different concentrations (10–60 mol%). The mixed powders were blended with deionized water then milled for 24 h. Subsequently, the solution was dried in an oven and sintered at 700–1,200°C for 1–8 h. Finally, the synthesized powders were ground, and the $ZnWO_4$ phosphor was prepared. The crystallization of the $ZnWO_4$ phosphor was improved by increasing the sintering temperature from 800°C to 1,200°C as seen in **Fig.15.** Meanwhile, the decreased FWHMs in the XRD patterns show that the grain size of the phosphor increased with the sintering temperature. Improvement in crystallization is normally accompanied by an increase in phosphor particle size. The particle sizes of $ZnWO_4$ phosphor were approximately 16.8, 17.9, 20.2, 19.6, 19.6, and 26.5 nm for sintering temperatures increasing in steps of 100°C from 700°C to 1,200°C, respectively. SEM result is consistent with the results of XRD analysis. Significant changes in

grain shape and size were observed with an increase in the sintering time. Optimal crystallization was realized in the case of the $ZnWO_4$ phosphor synthesized using 50 mol% WO_3 at 1,100°C for 3 h. The maximum emission intensity was achieved when the phosphor exhibited optimal crystallization.

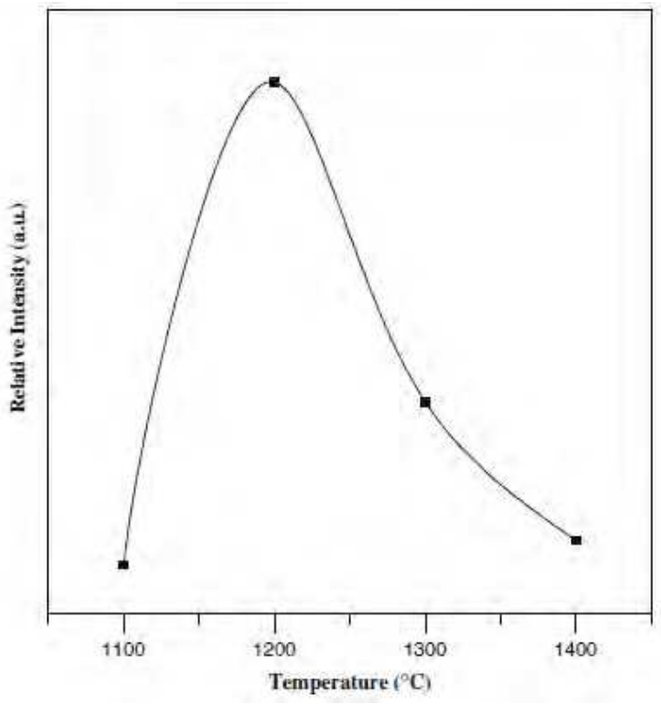

Fig. 14. The relative emission intensity versus the calcined temperature of $YInGe_2O_7$:5 mole% Eu^{3+} under an excitation of 393 nm. The signals were detected at 611 nm **[10].**

12. Phase change during sintering

Luminescence properties (both PL and TL) of Tricalcium phosphate (TCP) are very sensitive to its crystal phase (α/β). TCP crystals, in both α and β phases, were synthesized through two different routes, viz. wet precipitation and high temperature solid state reaction **[12].** The doping was done during the synthesis using suitable compounds of Dy and Eu. In the wet precipitation method used, the wet reaction is carried out using calcium nitrate and diammonium hydrogen phosphate in an ammoniated solution. The precipitation of tricalcium phosphate occurs through the chemical reaction $3Ca(NO_3)_2 + 2(NH_4)_2HPO_4 + 2NH_4OH \rightarrow Ca_3(PO_4)_2 + 6NH_4NO_3 + 2H_2O$. the supernatant liquid was decanted to collect the precipitate. It was then centrifuged thrice using distilled water and finely filtered. The filtrate was dried at 100°C in a hot air oven overnight and then calcined at 300°C in a muffle furnace for 3 h to remove any traces of other compounds. The calcined material was ground to form fine powder and graded using standard sieves. It was then sintered at high temperatures for 2 h in a programmable furnace to obtain the required phase (900°C for β-TCP and 1300°C for α-TCP). Various samples were prepared using dysprosium and europium as dopant. The doping was done by adding oxides of the dopant elements (dysprosium and europium) dissolved in minimum quantity of dilute nitric acid. The solid state synthesis of tricalcium phosphate was done through a high temperature firing of the

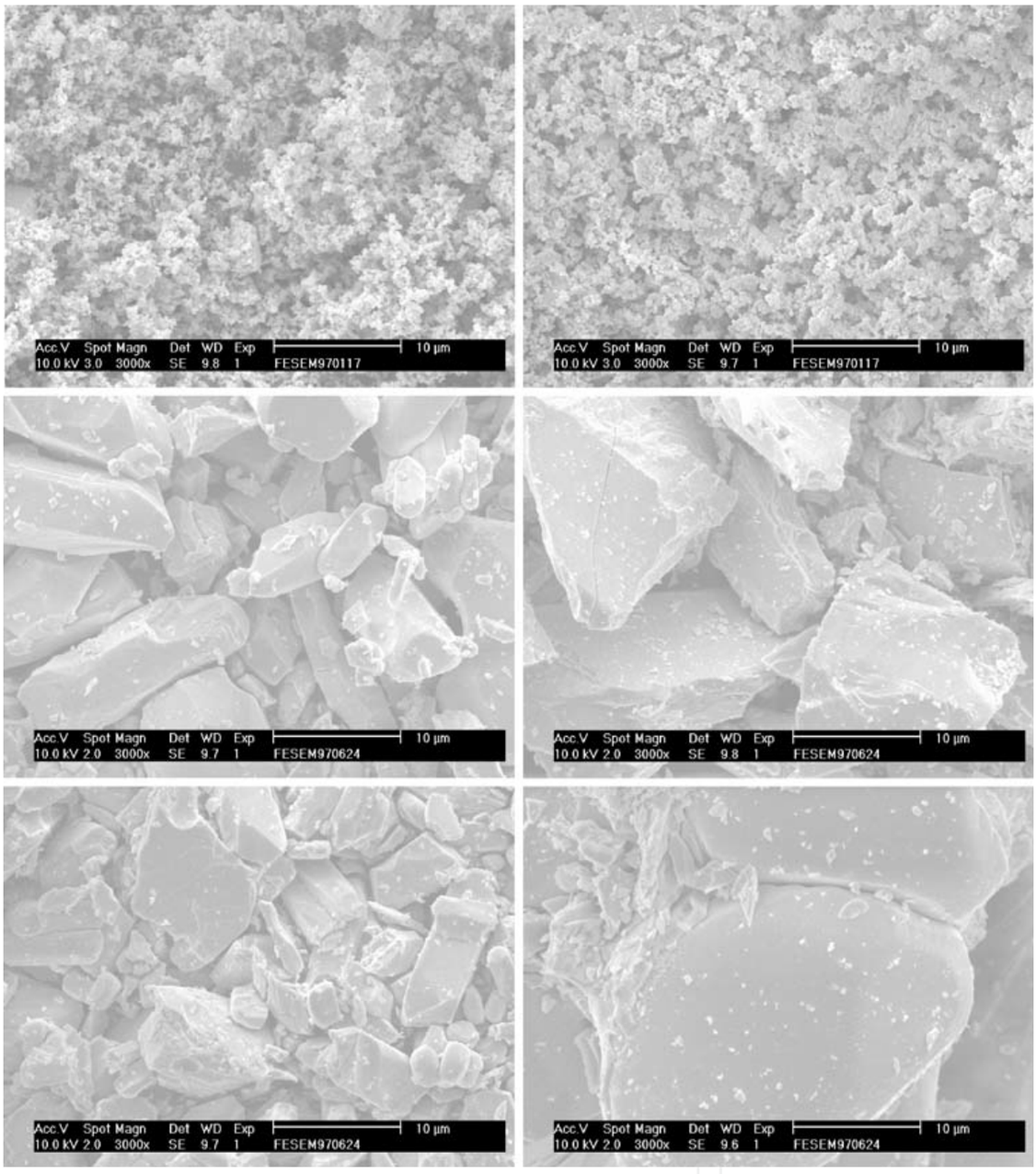

Fig. 15. Scanning electron microscope images of the $ZnWO_4$ phosphor prepared under different synthesis conditions; WO_3 concentrations at (a) 10 and (b) 50 mol% and sintered at 700°C for 3 h; WO_3 concentration at 50 wt% and sintered at (c) 1,100°C and (d) 1,200°C for 3 h; WO_3 concentration at 50 wt% and sintered at 1,100°C for (e) 1 and (f) 8 h **[11].**

powder mixture of calcium oxide (CaO) and dicalcium phosphate ($CaHPO_4$). The reaction governing the process is $CaO + 2CaHPO_4 \rightarrow Ca_3(PO_4)_2 + H_2O$. The dopant, in powder form, in appropriate amount was added to this, again mixed thoroughly for 1 h, and then transferred to a porcelain crucible. The powder was heated at about 300°C, then mixed for 1 h, and annealed at 1100°C for 2 h. The resulting compound was crushed to powder from

and graded using standard sieves. The samples prepared by wet precipitation annealed at 900°C) and by solid state sintering (annealed at 1100°C) techniques gave the spectra which match perfectly with that of β-TCP (Whitlockite mineral phase, JCPDS File No. 09-0169). The XRD pattern of sample prepared by wet precipitation method and annealed at 1300°C matched with that of α-TCP (JCPDS file number 09-0348). Though the TL efficiency of α-TCP is more compared to β-TCP, the former is less suited for TL applications as its peak temperature is on the lower side, which indicates high fading rate. An interesting outcome of the TL studies on doped tricalcium phosphate is that the phase transition from β to α during annealing could easily be identified through emission parameters. Dy is found to be an efficient dopant in β- TCP matrix compared to europium for maximum TL efficiency.

Aluminum oxide, commonly referred to as alumina, possesses strong ionic interatomic bonding giving rise to its desirable material characteristics. It can exist in several crystalline phases which all revert to the most stable hexagonal alpha phase at elevated temperatures. This is the phase of particular interest for structural applications. Alpha phase alumina is the strongest and stiffest of the oxide ceramics. Its high hardness, excellent dielectric properties, refractoriness and good thermal properties make it the material of choice for a wide range of applications. In a recent study, the α-alumina samples were prepared using a commercial ultra-pure γ-alumina powder obtained by thermal decomposition of ammonium alum ($NH_4Al(SO_4)_2$, $12H_2O$). The study of Zr, Th and Ca doping is performed through the impregnation of the γ-alumina powder by an alcoholic solution of zirconium or calcium chloride or of thorium nitrate **[13].** A further thermal treatment allows decomposition of the solvent and the salts (drying at 100°C for 24 h) and diffusion of the doping species inside the host material (600°C for 24 h). The doped γ-alumina is then transformed into doped α-alumina by a calcination at 1450°C for 2 h under a pure gas flow (O_2 or Ar+2% H_2). Th^{4+} and Zr^{4+} give rise to the same peaks on the glow curves, but the intensity is higher for Th^{4+}. For both dopants, the doping promotes shrinkage in the case of very low concentrations, in fact, until the cation integrates into the host material.

Carbon doped α-Al_2O_3 is a well known optically stimulated luminescence material used in radiation dosimetry **[14].** α-Al_2O_3 doped either with Tb^{3+} or Tm^{3+} has been prepared by combustion synthesis techniques for TL ionizing radiation dosimetry applications. In this method, the reactants (aluminum nitrate, urea and terbium or thulium nitrate) are ignited in a muffle furnace at temperatures as low as 500 °C. This synthesis route is an alternative technique to the conventional fabrication methods of materials based on α-Al_2O_3 (Czochralsky, Vernuil), where high melting temperatures and reducing atmospheres are required. After combustion, the samples were annealed at temperatures ranging from 1000 to 1400 °C for 4 h in order to obtain the pure α-phase structure and were then irradiated with a Co-60 gamma radiation source. The annealed samples present a well defined TL glow peak with a maximum at approximately 200 °C and linear TL response in the dose range 0.5–5 Gy. It was observed that a 0.1 mol% concentration of Tb^{3+} or Tm^{3+} and annealing at 1400 °C optimize the TL sensitivity. The highest sensitivity was found for Tm^{3+} doped samples which were approximately 25 times more sensitive than Tb^{3+} doped samples. These results strongly suggest that combustion synthesis is a suitable technique to prepare doped aluminum oxide material and that Tm^{3+} doped α-Al_2O_3 is a potential material for TL radiation dosimetry **[15].**

13. Sintering enhances thin film electroluminescence

$(Zn_xCd_{1-x})S$ phosphors are of considerable interest because of their use as window material in solar cells. While powder phosphors were prepared by heating at 900^0C in argon atmosphere, thin films (15-25 μm) were obtained by painting uniformly the mixture of phosphor powder along with 30% of $CdCl_2$ and 65% propylene glycol on SnO_2 substrate, drying in air at 120^0C for 2h and then sintering at 625^0C in N_2 atmosphere for 30 min. $CdCl_2$ is used as a sintering aid in the preparation of thin films of $(Zn_xCd_{1-x})S$. During sintering Zn is gradually replaced by Cd through the reaction $ZnS + CdCl_2 \rightarrow ZnCl_2 + CdS$. This is confirmed by the red shift in the optical absorption edge of thin film when compared to that of powder phosphor. In sintered films new centres are created which increases the luminescence efficiency and emission occurs in green, yellow-orange and red regions as against only yellow-orange emission in (Zn,Cd)S:Mn,Sm phosphors. While the 525 nm emission band was interpreted as due to free to bound transition from conduction band and acceptor band, the 625 nm emission band was attributed to the radiative recombination of electrons from the donor and acceptor levels. Excitation from Sm^{3+} ion can be transferred to donor-acceptor pair which leads to enhanced emission at 625 nm. In addition, new traps (donor levels) are created in ZnS type phosphors containing Cl^- as co-activator when Zn was gradually replaced by Cd. Moreover, during sintering, Zn vacancies (V_{Zn}) are created which act as deep acceptors.

14. Sintering in vacuum

While annealing Zr_2O in air at 1300^0C was accompanied with pronounced phase changes, phase composition remained unchanged even with prolonged holding at 1300^0C in vacuum. Vacuum sintering of powders with complex morphology at a high temperature thus allowed obtaining a dense ceramic based on Zr_2O_3 and Y_2O_3 with no monoclinic phase, despite the strong recrystallization of grains of the tetragonal phase.

15. Combustion synthesis

Self-propagating synthesis (SHS), also known as combustion synthesis, is a process that involves a reaction, which is sufficiently exothermic to sustain itself. This has led to a low cost, energhetically efficient method for the development of advanced materials. **Solution combustion synthesis (SCS)** is a promising method to prepare high-purity, small-sized and spherical particle phosphors because the starting raw materials are homogeneously mixed in liquid phases, and the high temperature generated instantly by exothermic reaction can volatilize low boiling point impurities leading to purer products. In addition, SCS results in products with narrow particle distribution because of the decrease in reaction time (a few seconds during the combustion reaction) **[16].** The mechanism of nanoparticle forming in SCS is shown in **Fig.16.** When heated rapidly at 550^0 C, the solution containing stoichiometric amount of redox mixture boils, dehydrate, followed by decomposition generating combustible gases. The volatile combustible gases ignite and burn with a flame. The large amount of escaping gases dissipates heat and thereby prevents the material from sintering and thus provides conditions for formation of nanocrystalline phase. Also, as the gases escape they leave voluminous, foaming and crystalline fine powder occupying the entire volume of the container and have no chance of forming agglomerations unlike in the other conventional processes. Therefore, in combustion synthesis, instantaneous and *in situ* very high temperature, combined with release of large volume of volatiles from liquid

mixture results in production of nanoparticles. The photographs in **Figs.17a and b** show the blue luminescence emission of as prepared (a) $BaMgAl_{11}O_{17}:Eu^{2+}$ and (b) $BaMgAl_{11}O_{17}:Mn^{2+}$ by solution combustion synthesis under UV illumination.

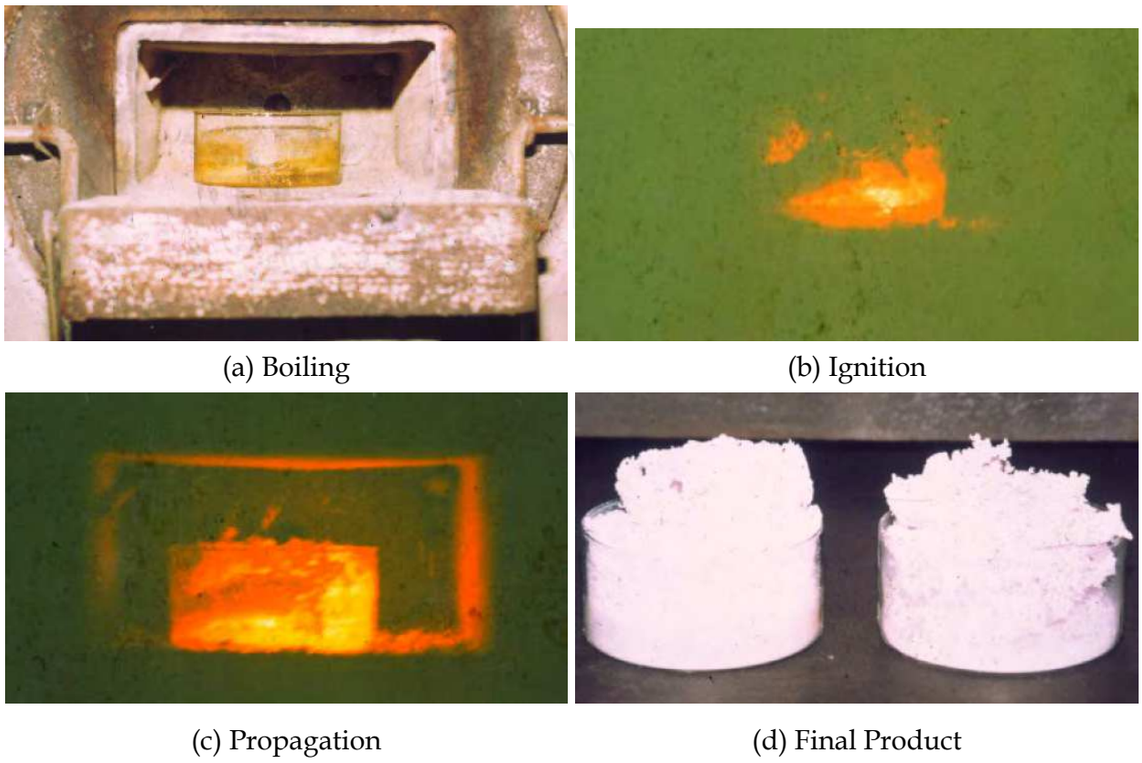

(a) Boiling (b) Ignition

(c) Propagation (d) Final Product

Fig. 16. Various steps in solution combustion process.

(a) (b)

Fig. 17. Photographs of as prepared (a) $BaMgAl_{11}O_{17}:Eu^{2+}$ and (b) $BaMgAl_{11}O_{17}:Mn^{2+}$ by solutiuon combustion synthesis show their blue luminescence emission under UV illumination **[17].**

Several luminescence phosphors have been successfully prepared by SCS technique. For instance, Ce-doped yttrium aluminum garnet (YAG, $Y_3Al_5O_{12}$) phosphor powders were synthesized using the combustion method. The luminescence, formation process, and structure of the phosphor powders were investigated by X-ray diffraction (XRD) analysis, scanning electron microscopy (SEM), and photoluminescence (PL) spectroscopy. The XRD

patterns show that the YAG phase can be produced with this method by sintering at 1000 °C for 2 h. This temperature is much lower than that required to synthesize the YAG phase using the conventional solid-state reaction method. No intermediate phases such as yttrium aluminum perovskite (YAP; $YAlO_3$) or yttrium aluminum monoclinic (YAM; $Y_4Al_2O_9$) were observed as a result of the sintering process. The powders were found to absorb excitation energies in the range of 410–510 nm. Furthermore, the crystalline YAG:Ce powder phosphor produced broad emission peaks in the range of 480–600 nm with the maximum intensity at 528 nm **[18]. Fig. 18** shows the TEM picture of BAM:Eu nano particles prepared by solution combustion synthesis [15].

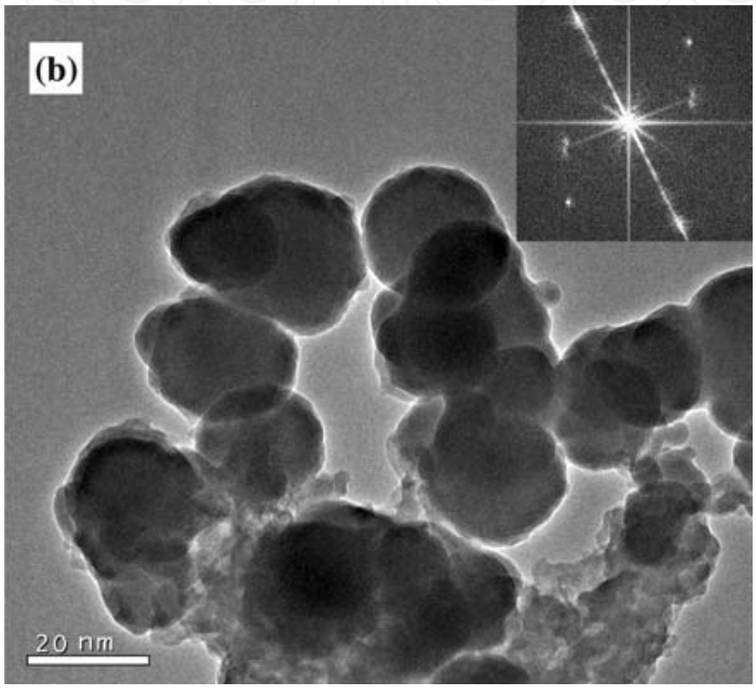

Fig. 18. TEM picture of BAM:Eu nano particles prepared by solution combustion synthesis [15].

16. Sol-gel method

The sol–gel process refers broadly to the room temperature solution routes for preparing oxide materials. The solutions of precursors are reacted to form the irreversible gels that dry and shrink to rigid oxide glasses and powders. Traditionally, phosphor films are generally deposited by using the sputtering technique and only in recent decades, the sol–gel method has been considered as a low cost alternative approach for the preparation of novel nano-structured materials including luminescent powders and films. The sol-gel route presents a lot of advantages: low-temperature synthesis, possible formation of powders with uniform grain morphology and achievement of homogeneous multicomponent films. An advantage in using the nano-crystalline phosphors is that non-radiative transition could significantly be controlled with a decrease in the crystal grain size. The preparation of the Zn_2SiO_4 precursor followed a simple route and was completed at room temperature and room humidity: firstly, $Zn(Ac)_2$ was dissolved in a mixture solution of de-ionized water and ethanol; secondly, stoichiometric TEOS was added into the above solution with agitation for

homogenization; thirdly, $Eu(Ac)_3$ and $Tb(Ac)_3$ were added into the precursor in the amount of 10 mol% ($Eu:Zn_2SiO_4$). Finally, a proper amount of 0.1M HCl was applied as catalyst for the hydrolysis of TEOS. The obtained precursor was transparent and clear, and was stable for several months if sealed at room temperature. Transparent gel can be obtained by leaving the precursor in air for about 2 or 3 days. Dry gel was prepared by baking the gel at 120^0C for 5 min. Powder phosphors were prepared by sintering the dry gel for 30 min at different temperatures from 650 to 850^0C. XRD data revealed that good crystallization of the powders could be obtained at about 850^0C, which is about 450^0C lower than that of the conventional solid-state reaction method **(Fig.19).** Phase analysis indicates that the obtained product has a willemite structure (rhombohedral). At the same time, a little amount of triclinic Zn_2SiO_4 was also detected. The TEM observation of the powders indicates that the particles are in the range 40–100 nm in diameter and have a good crystallinity.

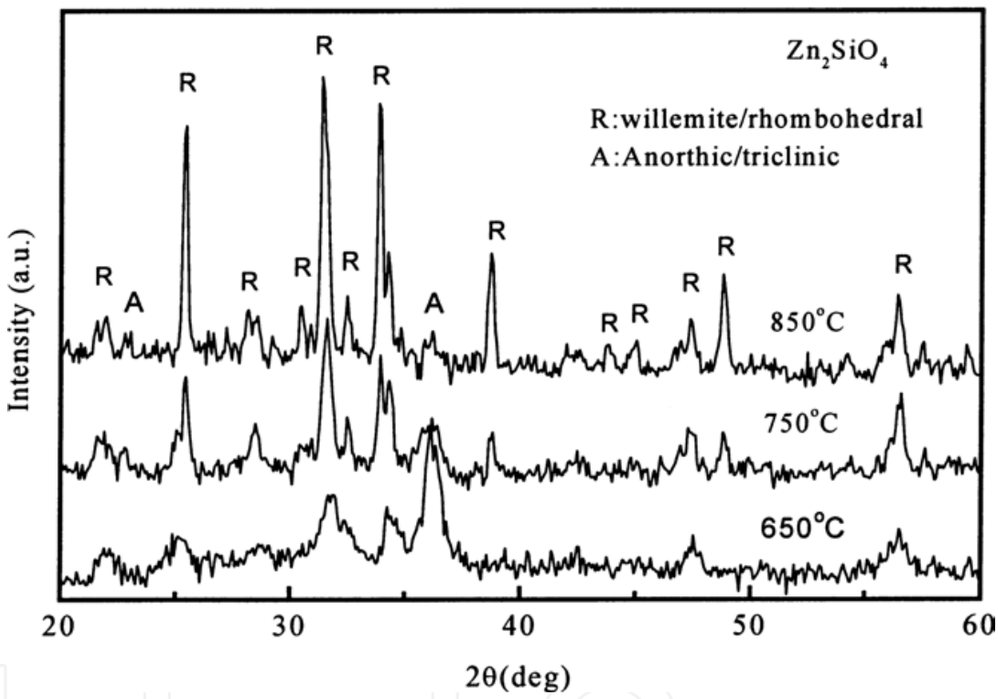

Fig. 19. XRD patterns of sol–gel derived Zn_2SiO_4 powders [19].

TG and DTA analysis in sol-gel route - In order to study the thermal decomposition of undoped xerogels, thermal gravimetry analysis (TGA) combined with infrared (IR) spectroscopy were used. TG and DTA (differential thermal analysis) results show cinetics of emitted gases during TG analysis, determined through the intensity evolution of the infrared main characteristic bands of each species. The total weight loss remains between -35 and -40% whatever the Tb^{3+} concentration is and occurs in three steps as shown in **Fig.20**. The first one (25–200°C) corresponds to the *departure of adsorbed moisture and chemically bonded alcohol molecules, i*n agreement with **Fig. 21.** This stage leads to a wide *endothermic peak*. The second and main weight loss (−19%) lying from 200 to 600°C is associated with an *exothermic phenomenon*. This stage can be *assigned to the pyrolysis of the organic parts* of the alkoxide groups and likely to more strongly adsorbed alcohol molecules. It is in good agreement with IR measurements which show that most of the residual organic groups are removed before

600°C. Above 600°C, only a weak weight loss takes place, ascribed to the withdrawal of the last residual alkoxy groups embedded in YAG matrix. Furthermore, *a sharp exothermic peak at about 894°C indicates the onset of YAG crystallization.* This is consistent with the XRD results

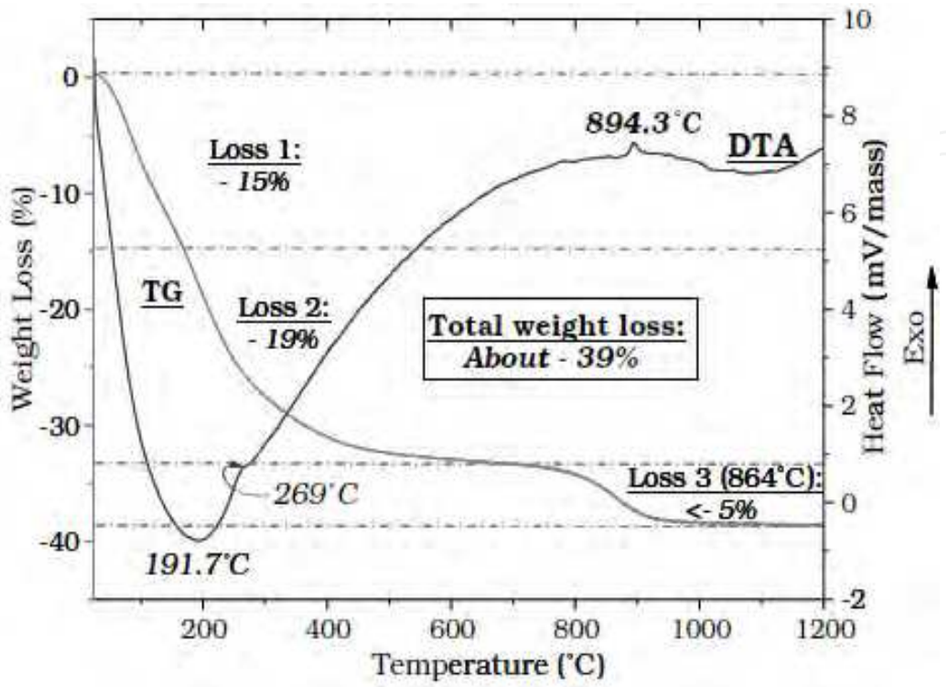

Fig. 20. TG and DTA profiles obtained fromYAG precursor gel **[20].**

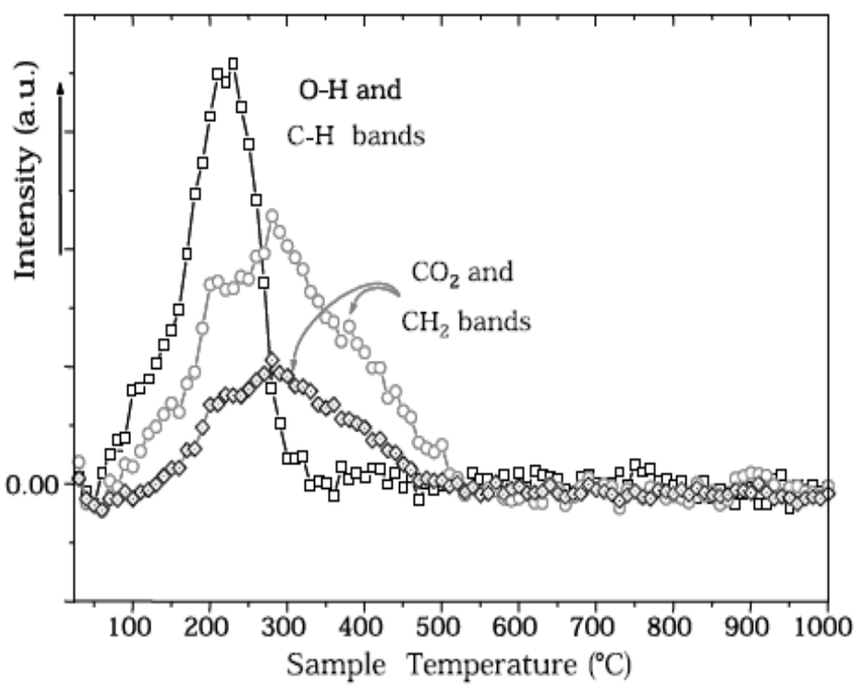

Fig. 21. Cinetics of gases emitted during TG analysis **[20].**

which showed that YAG sample begins to crystallize between 850 and 900°C. No significant weight loss appears thereafter, assuming the formation of the final product $Y_3Al_5O_{12}$.

17. Infrared spectroscopy

In the xerogel FTIR spectrum of of xerogel and undoped YAG sintered for 4 h at 1100°C, the presence of the characteristic organic bands is noticed. The broad band ranging from 2600 cm^{-1} to 3800 cm^{-1} is ascribed to −CH3 and −OH stretching in the isopropanol and alkoxy groups. This latter also involves −OH stretching resulting from water added in excess for hydrolysis and adsorbed from air moisture. A peak of weak intensity at about 2350 cm^{-1} is attributed to the adsorbed carbon dioxide from the atmosphere. The bands lying from 1200 to 1600 cm^{-1} are attributed to C-O and -CH_3 stretches bonds of organic groups whereas the peaks at about 1638 cm^{-1} is likely due to water added in excess to hydrolyze the heterometallic isopropoxide sol. Moreover, the several broad bands observed within the 400–850 cm^{-1} region of the IR spectrum correspond to M-O bonds (M=Y or Al) vibrations in YAG lattice. After sintering, specific bands related to the solvent and alkoxy groups significantly decrease or disappear. The carbon dioxide peak remains. Specific Al-O and Y-O vibrations peaks below 800 cm^{-1} are clearly identified as YAG ones.

18. Scanning electron microscopy

It is known that luminescent properties of a phosphor depend on its particles shape and size. On this account, the morphology of Tb^{3+} activated YAG samples has been studied by scanning electron microscopy (SEM). SEM micrographs of YAG:Tb^{3+}(5%) powder recorded at 800× magnification are shown in Fig.22. From the first picture related to the as-prepared xerogel **(Fig.22a),** it can be seen irregular size blocks. Voids and pores are also observed. The micrograph of heat-treated sample **(Fig.22b)** exhibits a denser network with fewer voids and narrow size distribution. For the two samples, the largest particles can reach several tens of micrometers.

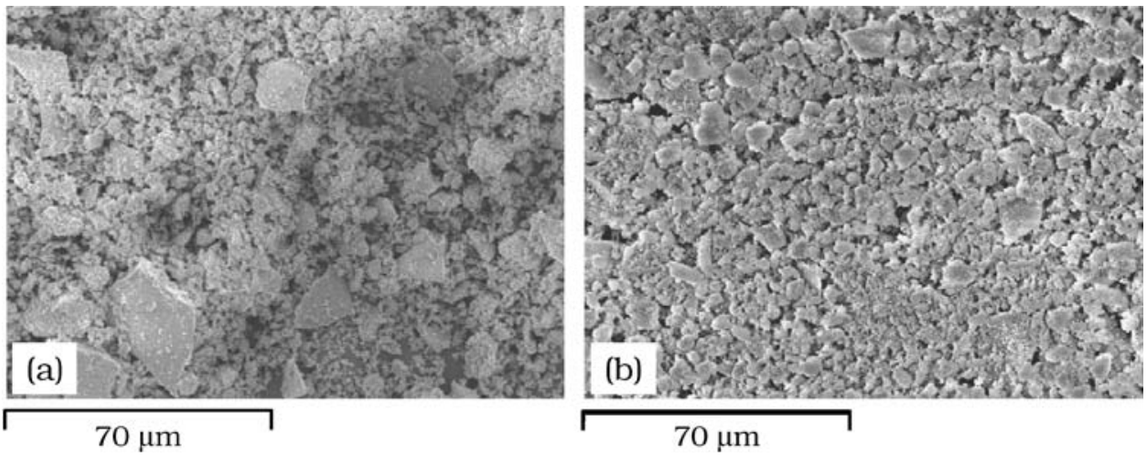

Fig. 22. SEM images recorded at 800× magnification from $Y_3A_{l5}O_{12}$:Tb^{3+}(5%) unheated (a) and annealed at 1100°C for 4 h (b) **[20].**

19. NMR

$Y_3Al_5O_{12}$ generally adopts a cubic garnet structure with lattice parameter of 12 Å (space group Ia¯3d). Its structure consists of a network where aluminum atoms reside both in octahedral and tetrahedral interstices whereas yttrium atoms occupy dodecahedral sites. Since the chemical shift of ^{27}Al NMR is sensitive to the local coordination, this technique is largely applied for checking the different phases and coordination states of Al centers in aluminates. As a result, MAS NMR ^{27}Al study has been undertaken on YAG samples in order to apprehend what kind of interatomic movements occur during sol-gel process. octahedral AlO_6 sites resonate between 15 and 30 ppm, the much less common AlO_5 sites between 40 and 25 ppm and tetrahedral AlO_4 between 80 and 50 ppm. On this account, the 2.6 ppm major resonance in the spectrum of the uncalcined xerogel corresponds to six-coordinate aluminum. Besides, two other distinct peaks located at about 35.4 and 61 ppm can be assigned to five and four-fold coordinated aluminum atoms. It can be noticed that the resonance at 35.4 ppm can also be consistent with a tetrahedral site distorted due to the presence of oxygen defects. ^{27}Al NMR spectral features of the sintered YAG powder reveal three signals at 0.426, 23.6 and 62.7 ppm, which can be imputed to the three types of coordination. The octahedral band has shrinked into the sharp signal at 0.426 ppm. Furthermore, since it has been demonstrated that Al atoms can only occupy tetrahedral and octahedral sites in crystallized YAG, we can deduce that the 35.4 and 23.6 ppm signals respectively in xerogel and crystallized powder correspond to distorted tetrahedral sites and not to five-fold coordinated one. Besides, by integrating peak areas, the ^{27}Al tetrahedral/octahedral ratio has been determined. Contrary to other studies, it remains the same after calcination, even if the resonance relative to "distorted tetrahedral" sites has weakened in favour of tetrahedral one **[20].**

20. Co-precipitation and sintering

The author has developed a simplified co-precipitation technique for the synthesis of $CaSO_4$:Dy TLD phosphor, which circumvent the cumbersome procedure, used so far, namely, evaporation of (highly corrosive) concentrated H_2SO_4 by recrysttalization. High TL sensitivity, uniform microcrystalline morphology, lower grain size (see SEM pictures shown below left) suitable for manufacturing dosimeters in solid form, better glow curve structure, lesser glow peak shift and better linearity and simplified preparation technique make the new phosphor a better alternative **(Figs.23 & 24).** The new recipe of $CaSO_4$:Dy based on co-precipitation technique is not only economical but also compatible for large scale production. Sintering of the co-precipitated phosphor at 700^0C in air increased its TL sensitivity by more than a factor of 2 (see TL glow curves shown below right) due to improved crystallinity and diffusion of Dy^{3+} ions from the surface to the whole volume of the grains as stated earlier.

In this experiment, initially, $CaSO_4.2H_2O$ and Dy_2O_3 salts were dissolved in hot concentrated H_2SO_4 acid and during slow dilution – water was added drop wise into the above hot solution – $CaSO_4$:Dy was found to precipitate. As per conventional solution chemistry, only $CaSO_4$ should precipitate since $CaSO_4$ does not dissolve in dilute H_2SO_4 acid. The Dy^{3+} ions should remain dissolved in the acid-water solution due to the high solubility of $Dy_2(SO_4)_3$ in water and in H_2SO_4 acid. The formation $CaSO_4$:Dy, as confirmed

by TL and PL studies, however indicated that a considerable amount of Dy ions present in the solution actually diffuse into the $CaSO_4$ host lattice during precipitation. This is considered as an amazing result which confirms that there is a competition between the solubility of Dy ions in $CaSO_4$ lattice and their solubility in acid solution. At low Dy concentrations (~ 0.1 mol%) normally used in TL phosphors, nearly 90% of Dy gets into the $CaSO_4$ lattice. Only at high Dy concentrations, the percentage of Dy getting into $CaSO_4$ lattice goes down.

21. Combustion and pyrolysis

A number of display phosphors has been recently synthesized in the author's laboratory using combustion and pyrolysis technique. In the pyrolysis technique, the constituent chemicals decompose and fuse by the action of heat at relatively low external temperatures (≤ 1000^0C) in air with adequate ventilation so that the gaseous products released during decomposition reactions escape and the fusion process is complete, Limitations of conventional solid state method are inhomogeneity of the product, formation of large particles with low surface area and hence mechanical particle size reduction is required, which introduces impurity and defects and presence of defects, which are harmful to luminescence. The problem of inhomogeneity could be mitigated by the use of non-conventional methods (wet-chemical) which include solution combustion. Combustion is an exothermic reaction and occurs with the evolution of heat and light. This method was accidentally discovered in 1988 in Prof. Patil's laboratory in India. The first synthesis of Eu^{3+} doped $LnBO_3$ (Ln=La, Gd and Y) borate phosphors by combustion method was made by his group. The emission spectrum of $LaBO_3:Eu^{3+}$ consisted of two bands at 615 and 595 nm and these bands were attributed to $^5D_0 \rightarrow {}^7F_2$ and $^5D_0 \rightarrow {}^7F_1$ transition of 9-coordinated Eu^{3+} ions, respectively. But, there were three bands at 625, 610 and 595 nm observed for $GdBO_3:Eu^{3+}$ and $YBO_3:Eu^{3+}$ phosphors. The band at 595 nm was attributed to magnetic dipole $^5D_0 \rightarrow {}^7F_1$ transition of Eu^{3+}, whereas the bands at 625 nm and 610 nm were attributed to electric dipole $^5D_0 \rightarrow {}^7F_2$ transition for 12 and 8 coordinated Eu^{3+} ions, respectively. Since electric dipole transition, $^5D_0 \rightarrow {}^7F_2$ depends upon the structure, two bands were observed for differently coordinated Eu^{3+} in $GdBO_3:Eu^{3+}$ and $YBO_3:Eu^{3+}$.

$(Y,Gd)BO_3:Eu^{3+}$ phosphor used in PDP displays was prepared earlier by combustion method using amino acetic acid as the combustion agent and then sintered at 1000 °C for 30 min. However, details of the recipe used and the PL sensitivity comparisons with commercial phosphor were not reported. In author's lab, raw materials used for the synthesis of $(Y,Gd)BO_3:Eu^{3+}$ and $YBO_3:Eu^{3+}$ phosphors using combustion technique were Y_2O_3, Gd_2O_3, H_3BO_3 and Eu_2O_3. NH_4NO_3 and urea (CH_4N_2O) were used as oxidizer (O) and fuel (F) respectively. The O/F ratio was kept at unity. After wet mixing in a porcelain crucible, combustion was carried out at 600 °C for 15 min in a muffle furnace with adequate ventilation so that the gaseous products released during combustion escape and the combustion process is complete. Combustion of the borate materials with urea fuel resulted in smoldering without flame. In contrast, with Oxalyl dihydrazide (ODH — $C_2H_6N_4O_2$) fuel, the combustion was reported to be flaming and the flame temperature measured using optical pyrometer was about 1400±100 °C. ODH process showed very sharp powder XRD pattern whereas urea process exhibited very broad powder XRD peaks. Therefore, by changing the fuel one could control particulate properties. However, ODH is nearly 50 times more expensive than urea

and hence we used only urea as the fuel in the combustion process. The material obtained after combustion was agglomerated and since it was not a hard material, a mild grinding in an agate mortar and pestle was found sufficient to remove the agglomeration which was then transferred to an alumina crucible before sintering at 1000 °C for 2 h in air in the furnace. The material obtained was once again hand ground mildly to obtain grain sizes below 30 µm. The grain morphology and their size distribution are being studied. The increase in emission intensity of the combustion synthesized red phosphors on calcination at high temperatures has been attributed to improved crystallinity. For PL intensity comparisons, $(Y,Gd)BO_3:Eu^{3+}$ PDP phosphor obtained from LG chemicals (Korea) was used.

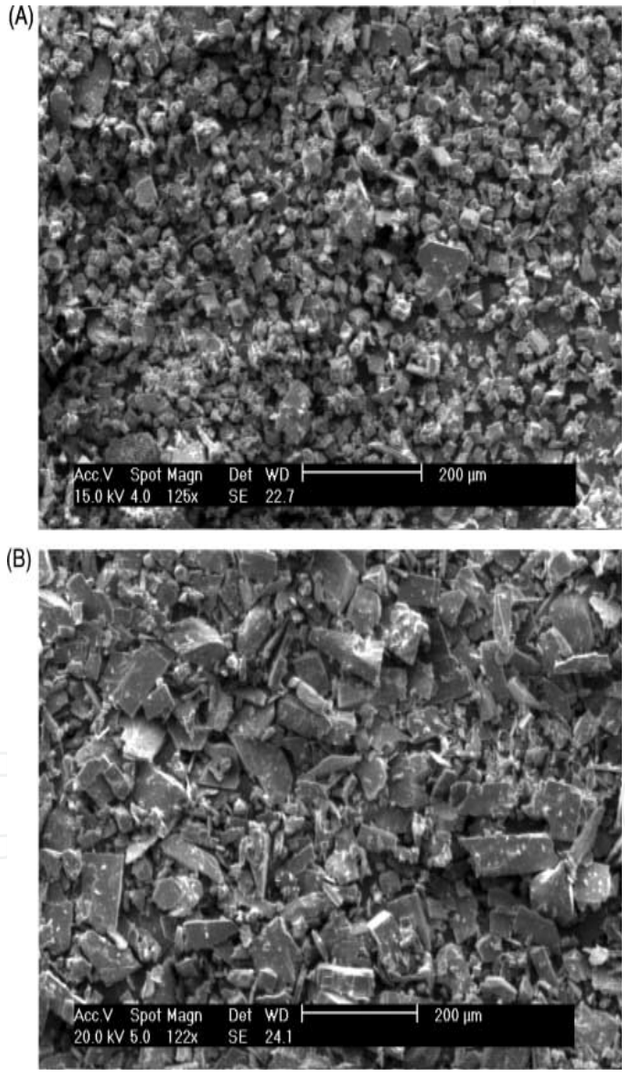

Fig. 23. SEM photographs of $CaSO_4$:Dy TL phosphor grains obtained by
(A) co-precipitation (in as-grown condition) and (B) conventional recrystallization (after grinding) **[21].**

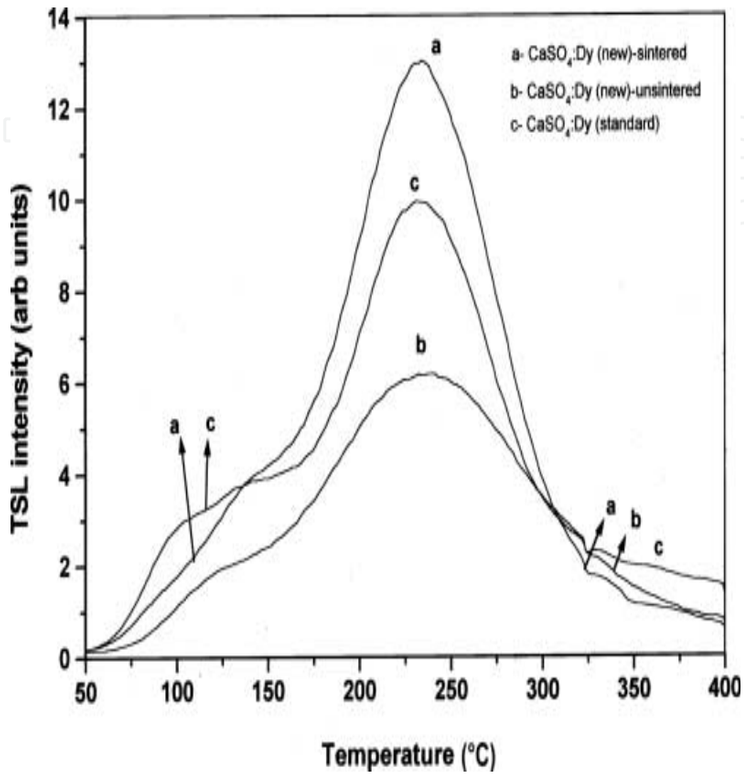

Fig. 24. Comparison of TL glow curves of $CaSO_4$:Dy phosphor obtained by recrystallization (c) and co-precipitation (a and b) The TL sensitivity of sample b increases by more than a factor of 2 on sintering at 700^0C for 1h **[21].**

The PL intensities of 592 nm emission peak on 393 nm excitation of $(Y_{0.54}Gd_{046})_x$ $(BO_3)_y$:Eu^{3+} (5 mol%) were found to vary with y/x molar ratio. Optimal PL efficiency is obtained at the y/x molar ratio of 1.38. XRD data reveal that at this molar ratio, interfering phases such as $(Y_{0.95},Eu_{0.05})_2O_3$ and $(Y,Eu)_3BO_6$ are negligible and H_3BO_3 had been fully used to build $(Y,Gd,Eu)BO_3$ crystal resulting in the maximized luminescence efficiency **(Fig.25).** A 12-fold increase in its luminescence efficiency was seen with an increase in Eu concentration from 0.5 to 8.4 mol%. No saturation or activation quenching of the PL efficiency was seen till the highest Eu concentration (8.4 mol%) level studied. PL efficiencies at still higher Eu concentrations are being studied. Interestingly, at 8.4 mol% Eu concentration, the PL sensitivity of $(Y_{0.54}Gd_{046})_x$ $(BO_3)_y$:Eu^{3+} is 40% higher than that of the commercial $(Y,Gd)BO_3$:Eu^{3+} PDP phosphor. It is concluded that $(Y_{0.54}Gd_{046})_x$ $(BO_3)_y$:Eu^{3+}, at the y/x molar ratio of 1.38, developed in this work is a potential candidate for application as a red phosphor for nUV LED.

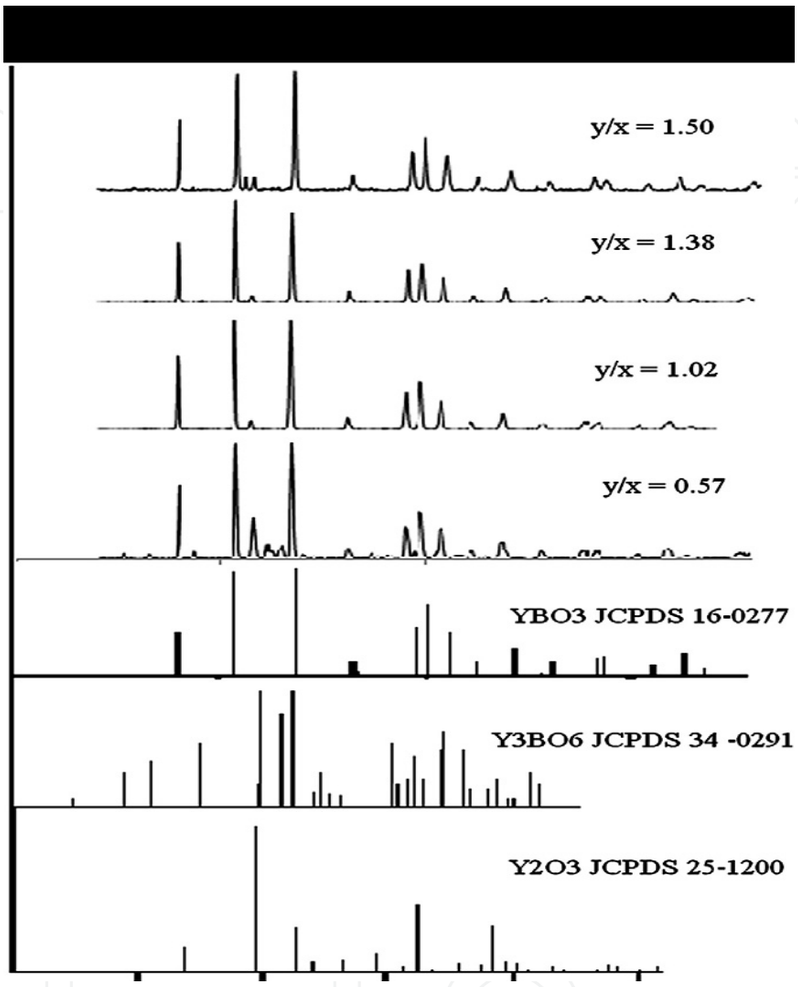

Fig. 25. XRD spectra of $(Y_{0.54}Gd_{046})_x$ $(BO_3)_y$:Eu^{3+} (5 mol%) sintered at 1000^0C as a function of BO_3 concentration. y/x ratio: 0.57, 1.02, 1.38 and 1.50. The standard XRD spectra of YBO_3 (JCPDS 16-0277), Y_3BO_6 (JCPDS 34-0291) and Y_2O_3 (JCPDS 25-1200) are also shown **[22].**

Development of high sensitive (Y,Gd)BO_3:Eu^{3+} phosphor also assumes significance since it is widely employed as red phosphor for plasma display panels (PDP) due to the BO_3 mediated energy absorption in the 130–170 nm VUV region giving rise to 593 nm emission. However the color purity of all YBO_3 based phosphors developed needs improvement since the 593 nm orange emission corresponding to the $^5D_0$–$^7F_1$ magnetic dipole transition is greater than the red components from electric dipole transitions in the 610–680 nm region. Studies carried out in this direction by others have succeeded only partially so far.**Fig. 26** shows luminescence from some of the phosphors prepared by pyrolysis.

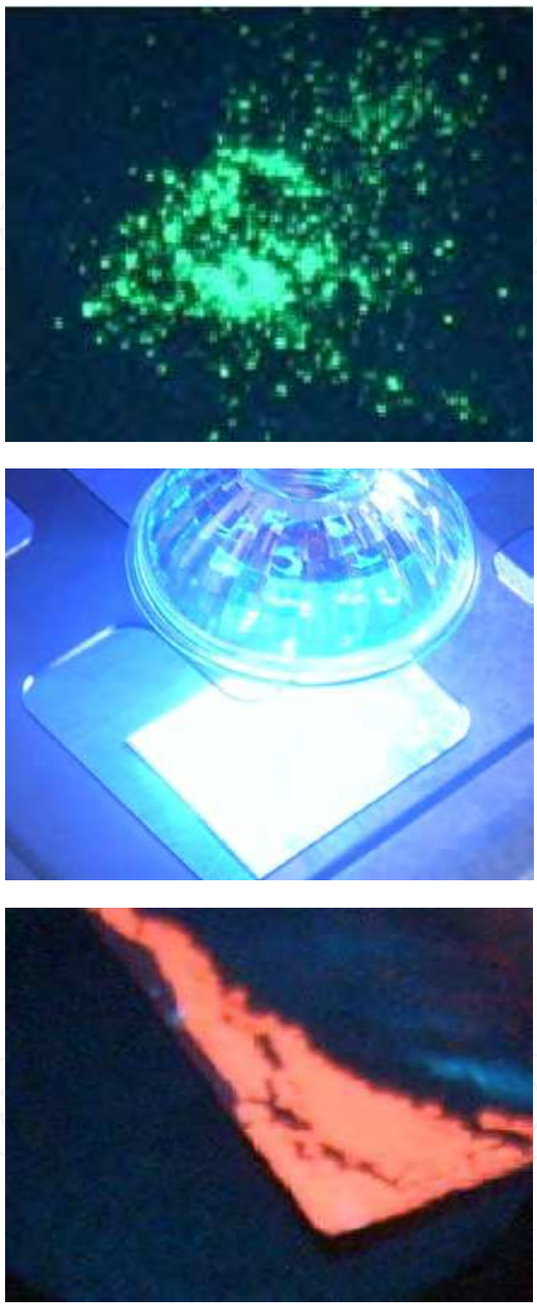

Fig. 26. Luminescence from some of the phosphors prepared by pyrolysis in author's lab are shown below under UV and 450 nm LED illumination. From left to right: Zn_2SiO_4:Mn, YAG:Ce LED and Y_2O_3:Eu^{3+}.

22. Microwave synthesis

Firing (sintering) is a necessary step for solid-state phosphor synthesis since activation energy must be supplied for the activators to go into the crystal structure of the host material. By solid-state reaction, conventional synthesis of phosphors takes many hours even with flux. Microwave processing is a relatively new technique and characterized by substantially accelerated reaction kinetics in the material systems if properly chosen. Using microwave processing, various phosphors have been synthesized. The high efficiency phosphors developed for field emission displays, plasma displays, and white light emitting diodes (LED) tend to be degraded by the operating environment and/or the devices' manufacturing conditions. Transparent oxide coating on phosphor powders is an effective approach to protecting phosphors from ageing, The coating can isolate the phosphor from the environment and could protect both the phosphor and the device. Microwave synthesis of some important phosphors and microwave processing of some phosphors coated with oxides are reported. In one study, microwave synthesis was carried out in a 2.45 GHz, 6 kW capability multimode microwave furnace with atmosphere controlled, although, only about 1 kW or less power was needed in the experiments. The powder sample (30-70 g each) was loaded in an alumina crucible, which was then placed in a properly insulated package with SiC as microwave susceptor. The insulation package was made of porous FiberFrax Duraboard 3000. The temperature of the sample was monitored with an optical pyrometer. The temperature was controlled by adjusting input power. During the microwave processing, the sample was rotating horizontally about the axis. The samples were microwave heated up and held at the designed temperatures for typically 10-20 min. The microwave-synthesized products were characterized for particle size, brightness, phase composition, morphology, luminescence emission, and color coordinates. Optimization of the parameters is required to achieve desired properties **[23].**

23. Spray pyrolysis

The aerosol processing, for example spray pyrolysis, is Known as a promising technique, especially to prepare the multi-component oxides like the $CaMgSi_2O_6$:Eu (CMS) phosphor. **Fig. 27** shows a simplified schematic diagram displaying the whole preparation steps of CMS phosphor by the spray pyrolysis. An ultrasonic aerosol generator with six vibrators (1.7 MHz) was used to atomize the precursor solution and the produced droplets were carried by the air (45 L min^{-1}) into a hot furnace with a quartz tube (length: 1200mm and inner diameter: 50 mm) at 900 °C. The formed particles were collected by a Teflon bag filter and posttreated at the temperature of 1000–1250°C for 5 h under a reducing atmosphere (5% H_2/N_2 mixture gas) for crystallization and activation of divalent europium. To test the thermal degradation, the prepared CMS and commercial BAM samples were mixed with commercially available binder paste (Daejoo corporation) which is practically used for the formation of phosphor films in PDPs. Next, the phosphor paste, wherein the fraction of powder was 50 wt.%, was fired at 500 °C for 30 min in the air environment. The crystal phase of the prepared CMS particles and PL were then analyzed.X-ray storage phosphors based on BaFBr:Eu are also made using this technique.

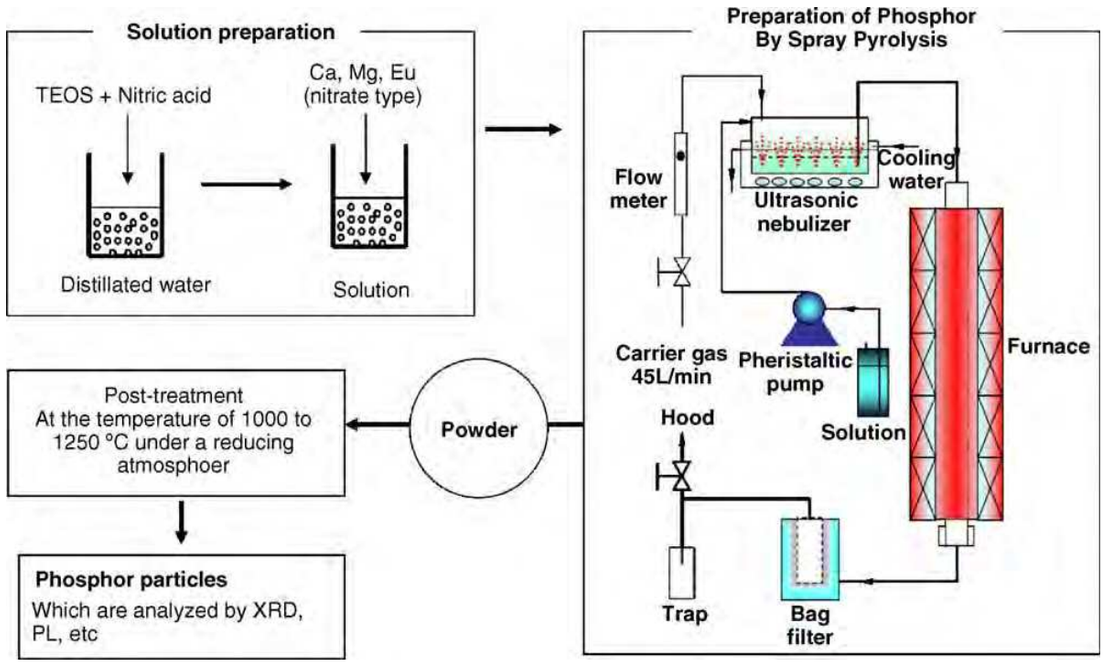

Fig. 27. Schematic diagram displaying the whole preparation steps of $CaMgSi_2O_6$:Eu blue phosphor particles by the spray pyrolysis **[24].**

24. Hydrothermal synthesis

The hydrothermal (HT) method, which uses autogenous pressure developed at temperatures above the boiling point of water, has been used especially in the synthesis of various ceramic oxide powders. The advantage of the hydrothermal method is that ceramic materials can be synthesized at relatively low temperatures (100-300˚C) without milling or calcinations [11]. The particle size and shape can also be controlled by various processing variables such as temperature, pH, and the addition of surfactants ormineralizers. The reaction is controlled by dissolution/precipitation of reactants in an aqueous medium. Therefore, the above processing variables are thought to have a significant influence on the dissolution or precipitation behavior, even though the exact roles or effects are not fully understood and differ in various systems.

For the hydrothermal synthesis, stoichiometric amounts of Gd_2O_3 and Eu_2O_3 were dissolved in 100 ml of distilled water acidified by the addition of nitric acid. After the complete dissolution of these oxides, NH_4OH solution was added drop wise until the pH of the solution reached 9. White precipitates were instantaneously formed and so-obtained precipitates were washed several times with distilled water by centrifugation. The washed precipitates were mixed with 50 ml solution of H_3BO_3 and distilled water. The amount of H_3BO_3 in the solution was adjusted so as to have an appropriatemole ratio with respect to Gd and Eu to give $GdBO_3$:Eu^{3+}. NH_4OH was used to adjust pH of the precursor solution to 7–10. After vigorous stirring, the precursor solution was placed in a Teflon-lined stainless steel autoclave with a volume of 100 ml. The solution was heated at 200-240˚C for 3–10 h" and cooled to room temperature. The resulting powders were filtered and washed several

times with distilled water by centrifugation, and finally suspended in ethanol then dried at 60°C for 5 h. An outline of the experimental procedure is shown in **Fig. 28.** For comparison, the bulk $GdBO_3:Eu^{3+}$ samples are prepared by a solid-state (SS) reaction at 500 and 1100^0C each for 2 h, respectively, from the mixture of Gd_2O_3, Eu_2O_3, and H_3BO_3 (20 wt.% excess).A high pH and excess H_3BO_3 promote the growth of $GdBO_3$ in a preferred orientation i.e., (2 0 0).

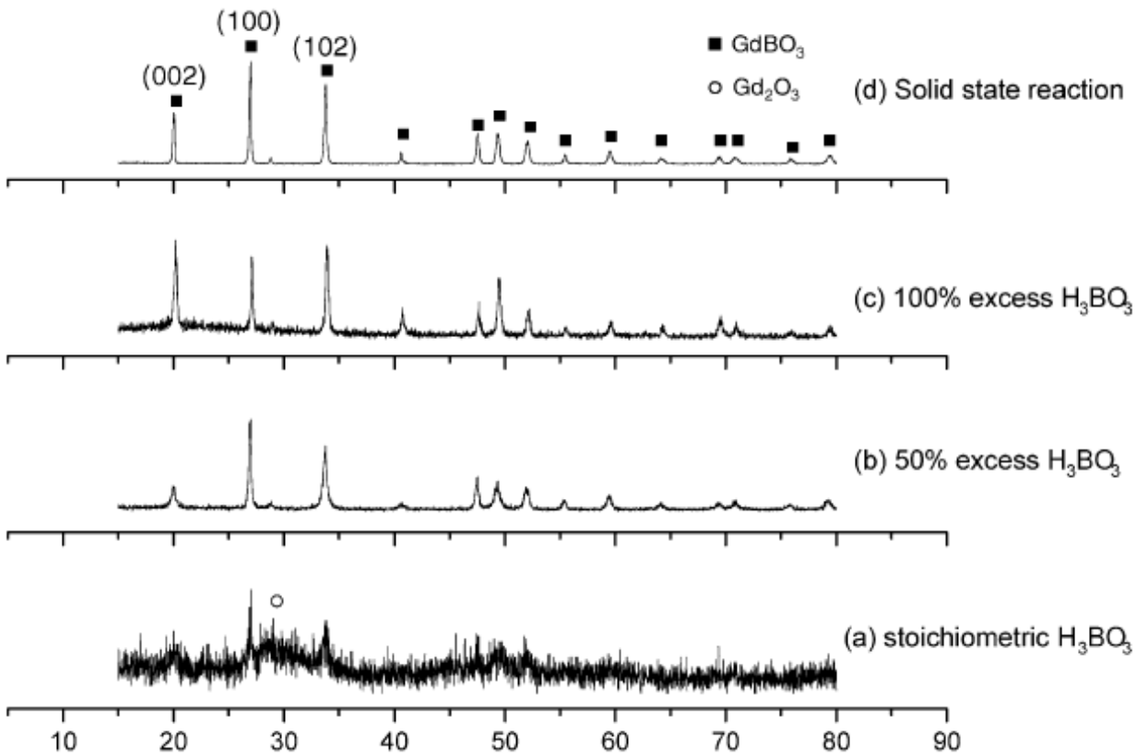

Fig. 28. XRD patterns of $Gd_{0.9}BO_3:Eu_{0.1}^{3+}$ powders synthesized with (a) stoichiometric, (b) excess amount of H_3BO_3, (c) by hydrothermal method (at 200^0C, 10h, pH8) and (d) by solid state reaction [25].

25. References

[1] Chun-Chieh Lin, Wei-Ren Liu, and Nae-Lih Wu. Effects of Sintering Fluxes on Structure and Luminescence of BaMgAl1O17:Eu2+ Phosphor. Abstract #2345, 218th ECS Meeting, © 2010 The Electrochemical Society

[2] L. Guanghuan , L. Tao , S. Yanhua, G. Guimei, X. Jijing, AN Baichao, G. Shucai and H. Guangyan. Preparation and luminescent properties of CaAl2O4:Eu3+,R+ (R=Li, Na, K) Phosphors. J. Rare Earths, Vol. 28, No. 1, Feb. 2010, p. 22

[3] W. B. Im, Y.I. Kim and D. Y. Jeon. Thermal Stability Study of BaAl2Si2O8:Eu2+ Phosphor Using Its Polymorphism for Plasma Display Panel Application.Chem. Mater., 2006, 18 (5), pp 1190–1195. DOI: 10.1021/cm051894v

[4] A R Lakshmanan, M T Jose, V Ponnusamy and P R Vivek kumar. Luminescence in CaSO4:Dy Phosphor – Dependence on Grain Agglomeration, Sintering Temperature, Sieving and Washing. J.Phys.D:Appl. Phys. 35, 386 (2002)

[5] C. Chang, Z. Yuan and D. Mao. Eu2+ activated long persistent strontium aluminate nano scaled phosphor prepared by precipitation method. Journal of Alloys and Compounds 415 (2006) 220–224

[6] A.R. Lakshmanan. Effect of pressure on the luminescence properties of gypsum, anhydrite, calcite and Dy doped CaSO4. Rad. Meas. 39, 235-240 (2005)

[7] Y. Wang, N. Can, P. Townsend. Influence of Li dopants on thermoluminescence spectra of CaSO4: with Dy or Tm. Luminescence in Rare-Earth Doped CaSO4 Phosphors. Rad. Meas. (in press)

[8] A.R. Lakshmanan. Photoluminescence and thermostimulated luminescence processes in rare-earth-doped CaSO4 phosphors. Prog. Mat. Science 44, 1-187 (1999)

[9] N.H. He and Y. Zhu. Improvement of morphology and luminescence of CaS:Eu2+ red emitting phosphor particles via carbon containing additive strategy. J. Mater. Sci. 43, 1515-1519 (2008)

[10] Y.S. Chang.The Effects of Heat Treatment on the Crystallinity and Luminescence Properties of YInGe2O7 Doped with Eu3+ Ions. Journal of Electronic Materials, Vol. 37, No. 7 1024-28 (2008)

[11] Su-Hua Yang & Fu-Shou Tsai & Jia-Xing Chen. Characterizations of white-light ZnWO4 phosphor prepared by blending complementary phosphor. J Solid State Electrochem. 14:937–943 (2010)

[12] K Madhukumar, H.K. Varma, M. Komath, T.S. Elias, V.Padmanabhan and C.M.K. Nair. Photoluminescence and Thermoluminescence properties of tricalcium phosphate phosphors doped with dysprosium and europium. Bull. Mater. Sci., Vol. 30, No. 5, October 2007, pp. 527–534.

[13] F. ferey, P. Grosseau, B. Guilhot, P. Iacconi and M. Benabdesselam. Thermoluminescence and sintering of high purity α- alumina doped by Zr, Th and Ca. Solid State Ionics, 2001, 141-2, 567-74.

[14] V. Schembri and B.J. Heijmen. Optically stimulated luminescence (OSL) of carbon-doped aluminum oxide (Al2O3:C) for film dosimetry in radiotherapy. Med. Phys.34(6) 2113-8 (2007)

[15] V.S.M. Barros, W.M. de Azevedo, H.J. Khoury, M.E.A. Andrade and P. Linhares Filho. Thermoluminescence study of aluminum oxide doped with terbium and thulium. Radiation Measurements. Volume 45, Issues 3-6, March-July 2010, Pages 435-437

[16] S. Ekambaram, K.C. Patil and M.J. Maaza. Synthesis of lamp phosphors: facile combustion approach, J. Alloys Comp. 393, 81 (2005)

[17] K.C. Patil, M.S. Hegde, T. Rattan and S.T. Aruna. Chemistry of nanocrystalline oxide materials:combustion synthesis, properties and applications. Advanced Ceramics. Pub. World Scientific, 2008, ISBN 9812793143

[18] S.K. Lee, H.H. Yoon, S.J. Park, K.H. Kim and H.W Choi. Photoluminescence Characteristics of Y3Al5O12:Ce3+ Phosphors Synthesized Using the Combustion Method with Various Reagents. Jpn. J. Appl. Phys. 46 (2007) pp. 7983-7986.

[19] H.X. Zhang, S. Buddhudu_, C.H. Kam, Y. Zhou, Y. L. Lam, K.S. Wong, B.S. Ooi, S.L. Ng, W.X. Que. Luminescence of Eu3+ and Tb3+ doped Zn2SiO4 nanometer powder phosphors. Materials Chemistry and Physics 68 (2001) 31–35

[20] A. Potdevin, G. Chadeyron, D. Boyer and R. Mahiou. Sol-gel elaboration and characterization of YAG:Tb3+ powdered phosphors. J Mater. Sci 41 (2006) 2201–2209

[21] A.R. Lakshmanan, M.T. Jose, O. Annalakshmi. Synthesis of high sensitive CaSO4:Dy TLD Phosphor by co-precipitation Technique. Radiat. Prot. Dosim. pp. 1-9 (2008) doi: 10, 1093/rpd/ncn 215.

[22] A,Lakshmanan, R.S. Bhaskar, Preema C. Thomas, R. Satheesh Kumar, V. Siva Kumar and M.T. Jose. A red phosphor for nUV LED based on (Y,Gd)BO3 :Eu3+. Mat. Letters 64, 1809-1812, 2010

[23] Kyeong Youl Jung, Hyun Woo Lee, Yun Chan Kang, Seung Bin Park,§ and Young Suk YangLuminescent Properties of (Ba,Sr)MgAl10O17:Mn,Eu Green Phosphor Prepared by Spray Pyrolysis under VUV ExcitationChem. Mater., 2005, 17 (10), pp 2729–2734 DOI: 10.1021/cm050074f

[24] Taehyung Kim, Shinhoo Kang. Hydrothermal synthesis and photoluminescence properties of nano-crystalline GdBO3:Eu3+ phosphor. Materials Research Bulletin 40 (2005) 1945–1954

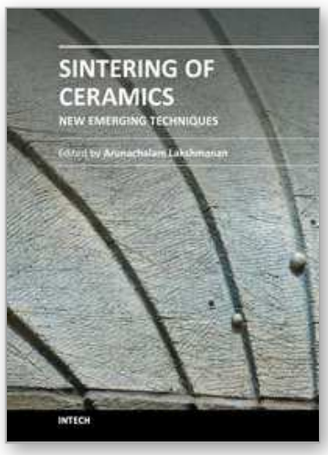

Sintering of Ceramics - New Emerging Techniques
Edited by Dr. Arunachalam Lakshmanan

ISBN 978-953-51-0017-1
Hard cover, 610 pages
Publisher InTech
Published online 02, March, 2012
Published in print edition March, 2012

The chapters covered in this book include emerging new techniques on sintering. Major experts in this field contributed to this book and presented their research. Topics covered in this publication include Spark plasma sintering, Magnetic Pulsed compaction, Low Temperature Co-fired Ceramic technology for the preparation of 3-dimesinal circuits, Microwave sintering of thermistor ceramics, Synthesis of Bio-compatible ceramics, Sintering of Rare Earth Doped Bismuth Titanate Ceramics prepared by Soft Combustion, nanostructured ceramics, alternative solid-state reaction routes yielding densified bulk ceramics and nanopowders, Sintering of intermetallic superconductors such as MgB2, impurity doping in luminescence phosphors synthesized using soft techniques, etc. Other advanced sintering techniques such as radiation thermal sintering for the manufacture of thin film solid oxide fuel cells are also described.

InTech Europe
University Campus STeP Ri
Slavka Krautzeka 83/A
51000 Rijeka, Croatia
Phone: +385 (51) 770 447
Fax: +385 (51) 686 166
www.intechopen.com

InTech China
Unit 405, Office Block, Hotel Equatorial Shanghai
No.65, Yan An Road (West), Shanghai, 200040, China
中国上海市延安西路65号上海国际贵都大饭店办公楼405单元
Phone: +86-21-62489820
Fax: +86-21-62489821

IntechOpen